Scientific paper

Investigation of the Corrosion Inhibition of Carbon Steel in Acidic Solutions by One Schiff Base: Experimental and Theoretical Studies

Djahida Haffar[1], Saida Mouzali[1,*], Linda Toukal[1], Youcef Bellal[2], Khadidja Boukerche[1], Abd El-Aziz S. Fouda[3]

[1] *Laboratory of Electrochemistry and Materials (LEM) Department of Engineering Process, Faculty of Technology, Ferhat Abbas University Setif-1, Setif 19000, Algeria*

[2] *Research Center in Industrial Technologies CRTI, P.O.Box 64, Cheraga 16014 Algiers, Algeria*

[3] *Chemistry Department, Faculty of Science, Mansoura University, Mansoura-35516, Egypt*

** Corresponding author: E-mail: mouzali2001@outlook.fr*
Tel: +213 774999252

Received: 01-10-2025

Abstract

Schiff base was synthesized and characterized, namely: 4-(1-(4-(dimethylamino)benzyl)-5-methyl-1*H*-benzo[d]imidazol-2-yl)-*N*,*N*-dimethylaniline (L). The molecular chemical structure of L was determined using ^{1}H NMR, FT-IR, UV-Vis spectroscopy, and elemental analysis. The performance and inhibition mechanism of compound L against the corrosion of carbon steel in 1 M HCl and 0.5 M H_2SO_4 were studied by the weight loss method and by electrochemical techniques (Tafel polarization and electrochemical impedance spectroscopy (EIS)). Outcome data obtained from these methods displayed that with increasing the concentration of compound L, its inhibition efficacy (η %) increases and reached 82.85% at 1×10^{-2} M, 25 °C using weight loss method. On the other hand, % η declined to 75.25% at the same concentration and at 55 °C. The polarization curves indicate that this compound behaves as mixed-type inhibitor. The adsorption of this compound was found to obey the Langmuir adsorption isotherm. The morphological appearance of the carbon steel surface of compound L using scanning electron microscopy (SEM) photos and atomic force microscopy (AFM) confirmed that compound L was adsorbed on carbon steel forming a film. The kinetic and thermodynamic parameters were calculated and discussed. Furthermore, the quantum chemical parameters were determined using the Density Functional Theory (DFT) method. This study confirms that there is agreement between experimental and theoretical results.

Keywords: Carbon steel; Corrosion inhibition; Density Functional Theory; Hydrochloric acid; Schiff base; Sulphuric acid.

1. Introduction

Carbon steel is a highly versatile material with numerous applications. Its excellent mechanical properties, low cost, and versatility make it an excellent choice for a variety of applications in chemical processing, building construction, fossil fuel processing, metal processing equipment, marine applications, nuclear fuel power plants, mining, pipelines, and petroleum refining production, among many other areas.[1] However, particularly in an acidic environment, its corrosion resistance is rather low.

Nonetheless, acidic environments are often used in a variety of industrial processes, including pickling, deposition, cleaning, and acidification of oil wells, all of which can severely corrode metallic surfaces.[2,3] Cleaning agents like sulfuric and hydrochloric acids are employed in a range of cleaning and rust removal procedures on the metal surface after operations are finished, exposing industrial equipment to corrosion. To prevent the metal from corroding in this situation, the corrosion protection model must be used.[4,5] Schiff bases have been the subject of numerous studies due to their interests in the industry.

Compounds containing a group >C=N- are known as imines or azomethines, but in general, they are known as "Schiff' bases" in honor of Schiff, who synthesized these types of compounds.[6] The advantages of these Schiff bases are mainly due to : i) their easy preparation process (they can be obtained in a single step) and were obtained in good yields, ii) their great thermal and photonic stability, as well as their incredible power of coordination in solution or the solid state, concerning the various acidic entities, both organic and metallic.[7] Due to these advantages, these compounds are applied in different fields of chemistry, namely, catalysis, liquid-liquid extraction, and corrosion, where they are used as inhibitors.[8–11] Corrosion inhibitors are an effective method for preventing metal corrosion. They have the originality of being the only means of preventing from the corrosive environment, which makes them easy to implement and an inexpensive method of corrosion control. Inhibitors have a very important role in the control of steel corrosion under acidic conditions.[12,13] Acidic conditions necessitate inhibitors having a polar group for attaching the molecule to the metal surface. Molecule size, orientation, and shape are critical parameters in corrosion inhibition.[14-16] Organic compounds are the most commonly employed inhibitors in acidic settings. The inhibitors initially adsorb onto the metal surface before impeding the corrosion reactions to reduce them.[17,18] According to the literature, in recent years, benzimidazole and its non-toxic derivatives are highly regarded in chemistry due to their impressive chelating abilities. Thus, they allow an effective inhibition of corrosion due to their powerful adsorption on the metal surface.[19,20]

The adsorption can take place using physisorption and chemisorption. This chemisorption adsorption type can happen when the inhibitor has free electron pairs and π electrons in the molecular structure.[21] The adsorption process, inhibitory efficiency, and inhibiting mechanism are influenced by the inhibitor's electrical and structural properties, surface type, temperature, reaction pressure, flow rate and the composition of the aggressive environment.[22,23]

Heterocyclic organic compounds have been found to be effective in inhibiting steel corrosion in acidic environments, such as 2-(2-pyridyl) benzimidazole (2PB),[24] 1-(4-methoxybenzyl)-2-(4-methoxyphenyl)-1H-benzimidazole,[25] 2-nonyl-1H-benzo [d] imidazole (NB), and 2-benzyl-1-hexyl-1H-benzo [d] imidazole (HB),[26] ionic benzimidazolium,[27] N,N'-bis(3-aminopropyl)piperazine (I1),N,N'-bis(3-(2-thenylidenimino)propyl) piperazine (I2), and its reduced form, N,N'-bis(3-(2-thenylamino) propyl) piperazine (I3), in inhibiting the electrochemical behavior of P460N in a 3.5 wt. % NaCl solution,[28] three morpholine-based compounds,N1-(2-morpholinoethyl)-N1-([pyridine-2-yl]methyl)propane-1,3-diamine (H1), 2-((3-(2-morpholinoethylamino)-N3-((pyridine-2-yl) methyl) propylimino)methyl)pyridine (H2), and N1-(2-morpholinoethyl)-N1,N3-bis(pyridine-2-yl methyl) propane-1,3-diamine (H3) were used as inhibitors for carbon steel corrosion in 0.5 M H_2SO_4 media,[29] and N1-(2-morpholinoethyl)-N1-((pyridine-2-yl)methyl)propane-1,3-diamine has been studied as a corrosion inhibitor for the protection of steel in acidic solution.[30] They are prevented by attaching to the metal surface through adsorption, facilitated by O, N-H, double bonds, conjugates, or aromatic rings in their chemical composition.

Similar studies have been carried out by several researchers who have reported the synthesis, identification, and the study of the anticorrosive effect of these ligands on steel in HCl medium. 2-(2-(4-chlorophenyl)-1H-benzo [d] imidazol-1-yl)-N-(p-tolyl)acetamide(CBIN-1),2-((2-(4-chlorophenyl)-1H)benzo[d]imidazol-1-yl)-N-(3,5-dimethylphenyl)acetamide (CBIN-2) and 2-(2-(4-chlorophenyl)-1H-benzo [d] imidazol-1-yl)-N-phenyl acetamide (CBIN-3),[31] 2-(1-(morpholinomethyl)-1Hbenzo[d]imidazol-2-yl) phenol (MBP), 2-(1-((piperazine-1-yl) methyl)-1H-benzo [d] imidazol-2-yl) phenol (PzMBP) and 2-(1-((piperidin-1-yl) methyl)-1H-benzo [d] imidazol-2-yl) phenol (PMBP)[32] and (2(-4 (chloro phenyl-1H-benzo [d] imidazol)-1-yl) phenyl) methanone (CBIPM).[33] The polarization curves demonstrate the benzimidazole derivatives exhibit mixed-type behavior and adhere to the Langmuir isotherm, on the steel surface by chemisorption and physisorption. The UV-visible electron absorption spectra after immersion time in aggressive environments confirm the formation of the complex of the compounds studied with Fe ions on the surface of the steel.

Quantum chemistry study confirmed the experimental results and showed that the studied inhibitors strongly tend to adsorption on the surface. On the other hand, Pournazari et al[34] studied the synthesis of a new inhibitor using a combination of benzene-1,2-diamine and benzaldehyde with $FeCl_3$ and use it as corrosion inhibitor for mild steel in a H_2SO_4 solution by electrochemical, chemical, quantum chemistry investigations, and optical microscopy at various temperatures. The efficiency reached to 97%, according to the electrochemical results. Optical microscopy shows reduced corrosion when using inhibitors. The quantum chemical analysis demonstrates that the benzene ring and the N atoms can be suitable sites for the adsorption on the metal surface.

Schiff bases have N atoms as their basic elements. Schiff base derivatives containing donor atom can act as good chelating agents for the transition of metal ions. Research shows that, Schiff bases and their metal complexes have been widely studied due to their import antiparasitic, fungicidal-bactericidal, and anticancer properties. Schiff bases are widely employed as catalysts, dyes, polymer stabilizers, pigments and corrosion inhibitors. The π or tridentate Schiff base ligands with transition metals form very stable complexes having medicinal applications.

Due to these advantages and the importance of Schiff bases, we propose to use the synthesized 4-(1-(4-(dimeth-

ylamino) benzyl)-5-methyl-1H-benzo[d]imidazol-2-yl)-N,N-dimethylaniline (L) as a corrosion inhibitor for carbon steel in HCl and H_2SO_4 solutions and to study its inhibitory power using weight loss, Tafel polarization and EIS techniques. A correlation between the molecular structure of this compound and the inhibitory activity was carried out using DFT and Molecular Dynamics Simulation (SDM) methods.

2. Experimental

2. 1. Synthesis of Compound L

4-(1-(4-(dimethylamino)benzyl)-5-methyl-1*H*-benzo[d]imidazol-2-yl)-*N*,*N*-dimethylaniline (L) was synthesized by a chemical condensation reaction as described in the literature.[35,36] In a 100 ml flask, we dissolved (1 mmol, 0.122 g) of an aromatic diamine (3,4-diaminotoluene) in 20 ml of absolute methanol while hot and stirred for 10 min. After complete solubility, one adds dropwise (2 mmol, 0.298 g) of aldehyde (4-dimethylaminobenzaldehyde) diluted in 20 ml of methanol (Scheme 1). The mixture is brought to reflux and stirring for 6 hours while maintaining the temperature of the solution at 60 °C. The products obtained in the form of a solid precipitate of yellow color are recovered by filtration under vacuum; the material was dried under a vacuum after being washed twice with hot methanol. The products are recovered with a yield of 60% and a melting point (mp) = 241 °C. Anal. Calc. for $C_{25}H_{28}N_4$: C, 78.12; H, 7.29; N, 14.59%. Found: C, 78.60; H, 7.07; N, 15.34%. IR (ν cm^{-1}): 1624 (C=N), 1550 (C=C), 1460 (C=C), 3036 (C-H); UV-Vis (Ethanol, λ_{max} nm): λ_{max} (269), λ_{max} (316); ^{1}H RMN (500 MHz, $CDCl_3$, **δ**ppm): 7.80 (d, J = 8.14 Hz, 1H), 7.64 (d, J = 8.67 Hz, 2H), 7.13-7.04 (m, 4H), 6.77-6.17 (m, 4H), 5.43 (s, 2H, CH_2), 3.03 (s, 6H, CH_3), 2. 97 (s, 6H, CH_3), 2.45 (s, 3H, CH_3).

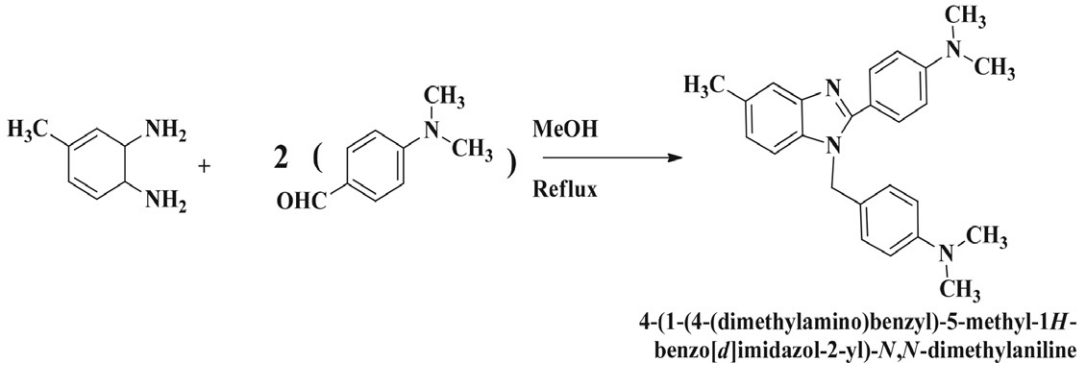

Scheme 1. Synthesis of 4-(1-(4-(dimethylamino) benzyl)-5-methyl-1H-benzo[d]imidazol-2-yl)-N, N-dimethylaniline (L).

2. 2. Spectroscopic Analysis

A Kofler Bank 7779 was used to determine the melting point of the ligand. Elemental analyses (C, H, S, N) were performed on a Perkin Elmer "2400 Elemental Analyzer". The IR spectra were collected with an FT/IR-JASCO 4200 instrument in the range of 500-4000 cm^{-1}. Electronic spectra were recorded on a UV spectrum in ethanol using a "U-650 JASCO spectrophotometer" with quartz cells. ^{1}H NMR measurements were taken at room temperature using a BRUKER Avance DPX250 Spectrometer (frequency is 250 mHz).

2. 3. Metal Samples

Carbon steel samples are composed of the following components: C 0.52-0.50%, Mn 0.5–0.80%, Si 0.40%, P 0.035%, S ≤ 0.035% and Fe being the balance. The carbon steel surface was sanded with abrasive papers before each measurement, with different grade sizes (500-800-1200-2000, and 2500 grade). The samples were washed many times with distilled water, treated with acetone to eliminate oil residue, dried with Josef's paper, and subsequently immersed in an experimental solution.

2. 4. Working Solutions

The Schiff base solutions (L) were prepared in aggressive electrolyte solutions of 0.5 M sulphuric acid (H_2SO_4 98%) and 1 M hydrochloric acid (HCl 37%). Freshly prepared medium was used for each experiment without stirring. A concentration range of 10^{-2} M to 10^{-6} M Schiff base (L) was used.

2. 5. Gravimetric Measurement

To investigate the effect of different concentrations, on the inhibitory potency of the test produit, carbon steel samples of 9.106 cm^2 are submerged in acid, both with and without adding inhibitor (L). The inhibitory effectiveness is assessed following a 6 hours immersion period at 25 °C. The gravimetric tests were performed in a 50 mL beaker. The volume of the electrolyte is 30 mL. They are immersed in the solution in an upright position. The experiments were set up in 6 different environments, one

was a control experiment and the other five experiments in which different concentrations of inhibitor L (10^{-6}, 10^{-5}, 10^{-4}, 10^{-3}, 10^{-2} M) in H_2SO_4 and HCl. Before any measurement, the surface condition of the sample includes abrading with the abrasive paper, washing with bidistilled water, degreasing with acetone, and drying under a flow of air. The sample is weighed on a ±0.0001 g precision balance and immediately added to the electrolyte. After soaking for 6 hours, the materials are extracted, rinsed with bidistilled water and acetone, dried, and weighed again.

2. 6. Electrochemical Measurements

Electrochemical tests were performed in an aerated environment without agitation using a VoltaMaster 4 software-controlled Voltalab 40. The setup included a cylindrical three-electrode cell with a volume of 200 mL and a double Pyrex glass top.

The reference electrode is a saturated calomel electrode (SCE), the counter electrode is a graphite rod, and the working electrode is a steel disc with a 0.19 cm^2 active surface area.

The polarization Tafel curves are plotted in a potential domain of (–700 to –300 mV/SCE) at a scanning speed of 0.5 mV/s at 25 °C. This low speed allowed us to carry out tests in quasi-stationary conditions. Before plotting the polarization curves, the electrode is held at its dropout potential for 30 min to attain steady state. The Tafel polarization technique studied the effect of temperature (25, 35, 45, and 55 °C) on the corrosion rate without and with varying levels of concentrations of L in HCl and H_2SO_4 medium. EIS measurements are conducted after 30 minutes of immersion in the acidic media. The sinusoidal voltage's amplitude is applied within the frequency range of 100 kHz to 10 mHz, with 10 points each decade.

2. 7. Scanning Electron Microscope Measurements

After about 6 hours of immersion in the two acid solutions without and with the optimum L concentration at room temperature, the surface morphology of the samples was analyzed with a miniature scanning electron microscope SEM (JEOL Neoscope JCM-5000).

2. 8. Quantum Chemical Data

Quantum chemical calculations of the compound studied (L) were analyzed to determine the correlation between the parameters derived from the compound's structure and the experimental corrosion inhibition results.[37] The DFT (B3LYP) was utilized using the 6-31G (d, p) basis set for the calculation, and the 09W Gaussian program.[38,39] The inhibitor L was geometrically optimized in both gas and aqueous phases.

The many molecular quantum characteristics, such as dipole moment (μ), absolute electronegativity (χ), absolute hardness (η), softness (σ), electron affinity (A), ionization potential (I), and energy gap (ΔE_{gap}), are defined by the following equations:[40–42]

$$A = -E_{LUMO} \tag{1}$$

$$I = -E_{HOMO} \tag{2}$$

The following equations are used to determine the overall hardness η and the chemical softness σ:

$$\eta = \frac{\Delta E_{gap}}{2} \tag{3}$$

$$\sigma = \frac{1}{\eta} \tag{4}$$

The global electrophilic index ω was introduced and is given by the following relation[43].

$$\omega = \frac{\chi^2}{2\eta} \tag{5}$$

where χ is the electronic chemical potential, such that:

$$\chi = \frac{I+A}{2} \tag{6}$$

This index evaluates the tendency of a chemical species to receive electrons. A lower value of μ, ω indicates a more reactive and effective nucleophile.

The calculation for the number of electrons transported (ΔN) was determined as follows:[44]

$$\Delta N = \frac{\chi_{Fe} - \chi_{inh}}{2(\eta_{Fe} + \eta_{inh})} \tag{7}$$

χ_{Fe} and χ_{inh} reflect the absolute electronegativity of iron and the inhibitor molecule, while η_{Fe} and η_{inh} imply the absolute hardness of iron and the inhibitor molecule, respectively. Theoretical values of χ_{Fe} = 7.0 eV and η_{inh} = 0 are employed to determine the quantity of transported electrons.[45]

$$\Delta E_{gap} = E_{LUMO} - E_{HOMO} \tag{8}$$

ΔE is the minimum energy for the excitation of an electron in a molecule. Consequently, high inhibitory efficacy results from a low value of ΔE. E_{HOMO} refers to the energy of the highest occupied molecular orbital, while E_{LUMO} represents the energy of the lowest unoccupied molecular orbital. The Molecular dynamic simulation (MDS) was performed using BIOVIA Materials Studio 8.0 software, marketed by Accelrys, Inc. USA.[46,47] In this study, we used three modules: First, the Forcite module is used to optimize the Examine the molecular structure of the inhibitor in the gas phase geometrically. The adsorption localization module was utilized to detect potential adsorption patterns. A simulation box measuring 17.38 × 17.38 × 27.16 Å

examines the interaction between the inhibitor molecule and the Fe (1 1 0) surface. Periodic boundary conditions were implemented in a three-dimensional space, and the equations of motion were included in the standard NVT ensemble. The simulation box included a Fe plate, a water plate with the inhibitor being studied, and a void layer. The experiment was performed at a temperature of 298 K using the COMPASS force field with nostril control.

3. Results and Discussion

3. 1. Elemental Analysis

The results obtained from elemental analysis of Compound L are in agreement with those calculated for the proposed formula.

3. 2. FT-IR Spectra

Among the most notable bands, characterizing the L Schiff base is the one corresponding to the azomethine groups. The band at 1624 cm^{-1} is attributed to the imine group.[48] Besides this primary function, the low-intensity bands observed in the 1439 and 1550 cm^{-1} region are due to the vibrations of the skeletons (C=C) in the plan and generally characterize the aromatic structures. The vibrations of the aliphatic C–H bonds are characterized by low intensity bands at 2917 and 3036 cm^{-1}.[49]

3. 3. UV-vis Analysis

The absorption spectra of compound L show an intense band at 269 nm attributed to the $\pi \rightarrow \pi^*$ transition of the aromatic rings, an intense band at 316 nm corresponding to the $n \rightarrow \pi^*$ transition of the imine group.[50]

3. 4. ^{1}H RMN Analysis

The computed chemical shifts corresponding to the molecule are obtained from the $CDCl_3$ solution. The 1H NMR spectrum of compound L shows the disappearance of four ethylenic NH and CH protons of the imine, confirming the presence of a heterocyclic group. We also note the appearance of a singlet at 5.43 ppm due to the proton of the -CH_2- group, while the methyl groups resonate in the form of three singlets between 3.03 and 2.45 ppm. The aromatic protons resonate between 7.80 and 6.17 ppm.[51–53]

3. 5. Gravimetric Measurement

The weight loss method was used to investigate the inhibition performance of L at 25 °C and at various concentrations of inhibitor L at 25 °C and at various concentrations of inhibitor L in both HCl and H_2SO_4 media. This method measures the mass loss Δm of the sample contact surface (s) with the medium during the immersion time (t). The corrosion rate (W_{corr}) was determined using equation (9):

$$W = \frac{\Delta m}{s.t} \quad (9)$$

$\Delta m = m_i - m_f$, Δm: Mass loss in mg. m_i: initial mass in mg before immersion, m_f: Final mass in mg after the sample has been immersed in the solution for a time t, s: surface area in cm^2 t: Time in hours. The inhibitory efficacy (η_w) of a compound is calculated by the relationship (10):

$$\eta_w(\%) = \frac{W_0 - W_i}{W_0} \times 100 \quad (10)$$

w_0 and w_i reflect the corrosion rates without and with the compound respectively.

The W_{corr} (mg cm^{-2} h^{-1}) and inhibitory efficacy η_w were found gravimetrically for a 6-hours immersion period of compound L at various concentrations compared to the corrosion of carbon steel in HCl and H_2SO_4 at 25 °C (Table 1).

Table 1. Corrosion parameters of carbon steel in HCl and H_2SO_4 without and with different concentrations of inhibitor L from gravimetric measurements at 25 °C for 6 h.

Inhibitor	Acid solution Concentration (M)	HCl W_{Corr} (mg cm^{-2} h^{-2})	HCl η_w (%)	H_2SO_4 W_{Corr} (mg cm^{-2} h^{-2})	H_2SO_4 η_w (%)
	Blank	0.2397	–	0.2800	–
	10^{-6}	0.0988	58.00	0.1881	32.67
L	10^{-5}	0.0878	63.24	0.1611	42.47
	10^{-4}	0.0750	68.60	0.1090	60.77
	10^{-3}	0.0585	75.49	0.0677	75.81
	10^{-2}	0.0420	82.38	0.0347	87.58

These results indicate that the tested compound L inhibits steel corrosion in the environment. Its inhibitory efficacy increases with increasing inhibitor concentration.[54]

This behavior is due to the significant adsorption of inhibitor L on the carbon steel surface in acidic media. At a 10^{-2} M the inhibitory efficiency of H_2SO_4 is greater than that of HCl.[55]

The results are due to the spontaneous reactivity of steel (ferritic steel) in acidic conditions, resulting in the release of hydrogen and metal oxidation processes. Compound L in an acidic environment hinders the reduction and oxidation reactions that cause steel deterioration; hence, higher L concentrations enhances the adsorption of molecules of inhibitor L onto the metal surface.

Fig. 1 presents the evolution of W_{corr} and η_w of carbon steel in HCl and H_2SO_4 for 6 hours as a function of the concentration of compound L. Increasing the concentration of L decreases the corrosion rate and increases the inhibitory efficacy, as indicated from the data.

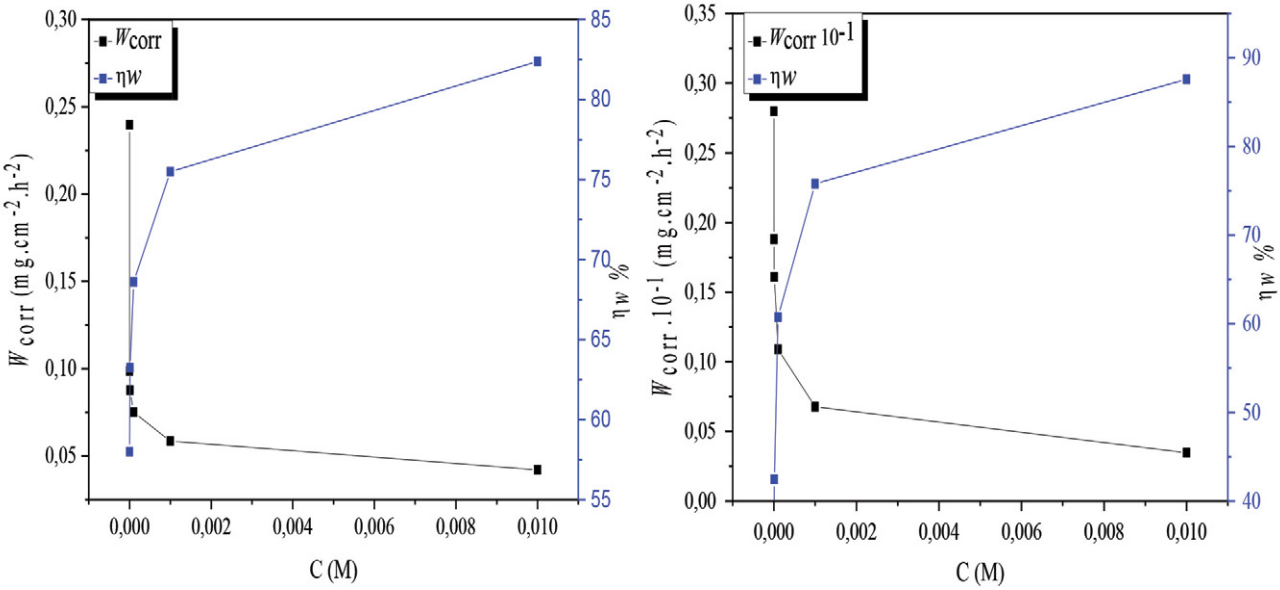

Figure 1. The graphs show the variation of the inhibition efficiency and the corrosion rate as a function of the concentration of the compound L in HCl and H_2SO_4 at 25 °C.

Table 2. Inhibition rates of carbon steel in HCl and H_2SO_4 solutions with and without the addition of 10^{-2} M of compound L as a function of immersion duration.

	t = 06 hours		t = 168 hours		t = 336 hours		t = 504 hours		t = 672 hours	
	Δm (g)	R_{inh} (%)	Δm (g)	R_{inh} (%)	Δm (g)	R_{inh} (%)	Δm (g)	R_{inh} (%)	Δm (g)	R_{inh} (%)
H_2SO_4	0.1333	–	0.168	–	0.3744	–	0.4154	–	0.5901	–
H_2SO_4 + L	0.0911	31.65	0.1473	12.32	0.1615	56.86	0.1669	59.82	0.1768	70.04
HCl	0.0016	–	0.0392	–	0.0739	–	0.0898	–	0.1077	–
HCl + L	0.0011	31.25	0.0317	19.13	0.0409	44.65	0.0449	50.00	0.0538	50.04

Gravimetric measurements were obtained using the optimum 10^{-2} M concentration of compound L in aggressive HCl and H_2SO_4 media at 25 °C and at different immersion times (6–672 hours). Parameters such as Δm and the inhibition rate of carbon steel in HCl and H_2SO_4 are summarized in Table 2. The inhibition rate) is obtained from equation (11):

$$R_{inh}(\%) = \left(\frac{\Delta m}{m_i}\right) \times 100 \quad (11)$$

The weight loss of carbon steel varies proportionally and slightly with the immersion time in HCl and H_2SO_4 with compound L compared to without addition (Fig. 2a). This behavior could be attributed to the significant adsorption and formation of a durable layer of compound L on the surface of the carbon steel. On the other hand, Fig. 2b shows that the inhibition rate of carbon steel increases progressively with the immersion time and that the best inhibition results are obtained in the H_2SO_4 medium (70.04%) than in the HCl medium (50.04%). These results showed that HCl reacts less aggressively than H_2SO_4. So, inhibitor L can retard metal corrosion by covering the carbon steel surface with a thin film, thus reducing weight loss.[56]

3. 6. Tafel Polarization Neasurements

Figs 3a, b shows the Tafel polarization curves of carbon steel in HCl (a) and H_2SO_4 (b) at varying concentrations of inhibitor L at 25 °C

The results showed that the presence of compound L resulted in lower current densities at the anode and cathode in both media.

The inhibition efficiency η_P (%) was calculated from the polarization curves using the equation (12):

$$\eta_P\% = \left(\frac{i^{\circ}_{corr} - i_{corr}}{i^{\circ}_{corr}}\right) \times 100 \quad (12)$$

where i°_{corr} and i_{corr} are the current densities extrapolated from the anodic and cathodic Tafel curves after a 30 minute immerse in HCl or H_2SO_4 at 25 °C, respectively, without and with the inhibitor added. The different corrosion parameters of compound L in HCl and H_2SO_4 at 25 °C, such as E_{corr} (mV/SCE), i_{corr} (mA cm^{-2}), cathodic Tafel

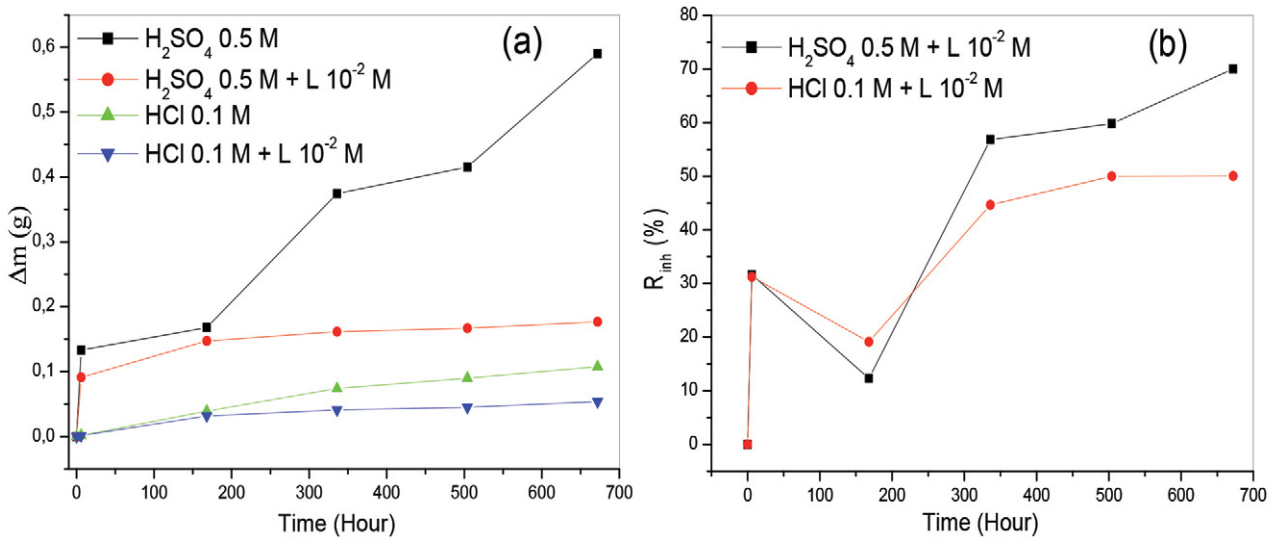

Figure 2. Mass loss (a) and inhibition rate (b) of carbon steel in HCl and H_2SO_4 as a function of immersion time, with and without L 10^{-2} M at 25 °C.

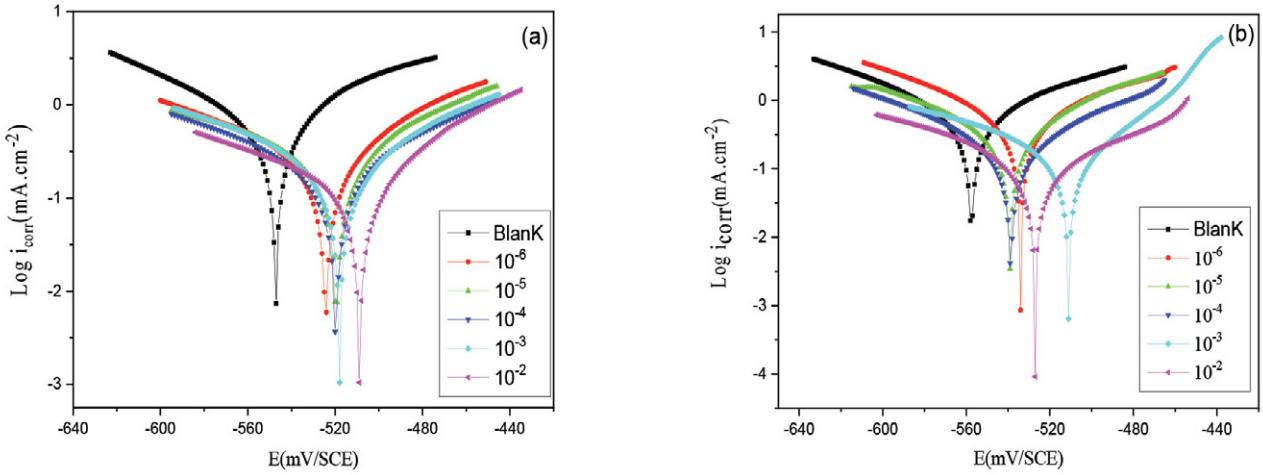

Figure 3. Tafel curves for carbon steel at altered concentrations of compound L in HCl (a) and H_2SO_4 (b) solutions.

Table 3. Corrosion parameters of carbon steel at 25 °C in HCl and H_2SO_4 at different concentrations of compound L, determined by plotting polarized curves.

	Concentration (M)	$-E_{corr}$ (mV/SCE)	i_{corr} (mA.cm^{-2})	b_a (mV/dec)	$-b_c$ (mV/dec)	θ	η_p (%)
HCl	blank	547.6	0.60	81.4	97.2	–	–
	10^{-6}	523.0	0.24	77.4	113.4	0.60	60.2
	10^{-5}	520.9	0.21	76.0	115.1	0.65	65.1
	10^{-4}	519.8	0.19	94.9	122.4	0.68	68.3
	10^{-3}	518.0	0.16	73.4	90.2	0.73	73.3
	10^{-2}	508.9	0.12	57.2	107.3	0.80	80.3
H_2SO_4	blank	557.2	0.70	116.1	100.4	–	–
	10^{-6}	534.0	0.44	84.1	78.0	0.37	37.14
	10^{-5}	539.2	0.31	72.2	90.1	0.56	55.71
	10^{-4}	538.7	0.24	91.3	95.8	0.66	65.71
	10^{-3}	511.1	0.18	44.8	117.1	0.74	74.28
	10^{-2}	527.0	0.12	113.7	106.0	0.83	82.85

slopes b_c (mV/dec), anodic Tafel slopes b_a (mV/dec) and The inhibitory efficacy η_P (%) for various concentrations are presented in Table 3.

The corrosion current density (i_{corr}) values decreased with increasing concentration of compound L, from 0.6 mA cm^{-2} to 0.12 mA cm^{-2} in 1 M HCl and from 0.70 mA cm^{-2} to 0.12 mA cm^{-2} in 0.5 M H_2SO_4. Note that $b_c > b_a$ means that the cathode is more polarized, and the kinetics of dissolution of the steel is limited by the cathodic reaction of the proton discharge at the metal surface. The cathodic and anodic polarization curves indicate that the addition of compound L decreases the corrosion current densities and slightly modifies the values of E_{corr}. The results confirm that compound L acts as a mixed-type inhibitor, since the shift of the E_{corr} in the different concentrations of compound L is less than 85 mV compared to the corrosion potential without inhibitor.[57] Consequently, the values of η_p (%) increase with increasing concentration of compound L, reaching a maximum value of 82.85% and 80.3% at 10^{-2} M for H_2SO_4 and HCl, respectively.[58]

The results show that the presence of compound L reduces the anodic dissolution of Fe^{2+} and slows down the evolution of the H^+ ion discharge, which can be explained by the presence of an adsorption film on the metal surface; on the other hand, in the cathodic region, the curves show parallel Tafel lines, suggesting that the reduction of H^+ on the steel surface obeys a pure activation mechanism. This compound L effectively inhibits steel corrosion in both H_2SO_4 and HCl solutions. This suppression is likely caused by an electron-donating group within its chemical composition. The presence of non-binding electron pairs on nitrogen atoms and π electrons in aromatic rings can lead to conjugation that facilitates the adsorption of the inhibitor.[59,60]

3. 7. EIS Tests

Fig. 4 shows the Nyquist and Bode plots obtained at open circuit potential after immersion for 30 minutes in HCl and H_2SO_4 solutions at 25 °C, both with and without

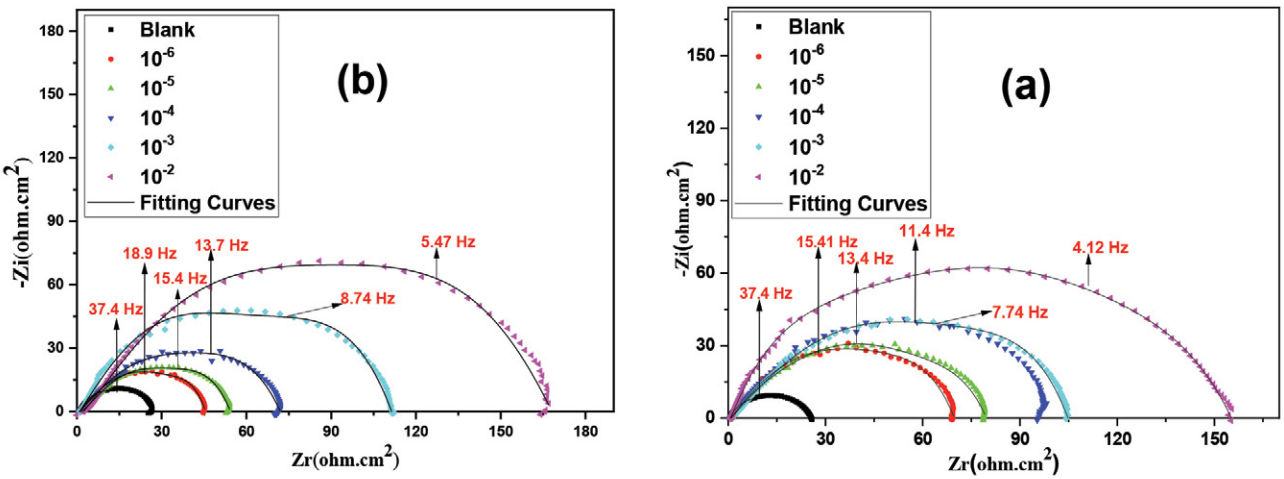

Figure 4. Nyquist plots of carbon steel in HCl (a) and H_2SO_4 (b) at various concentrations of compound L at 25 °C.

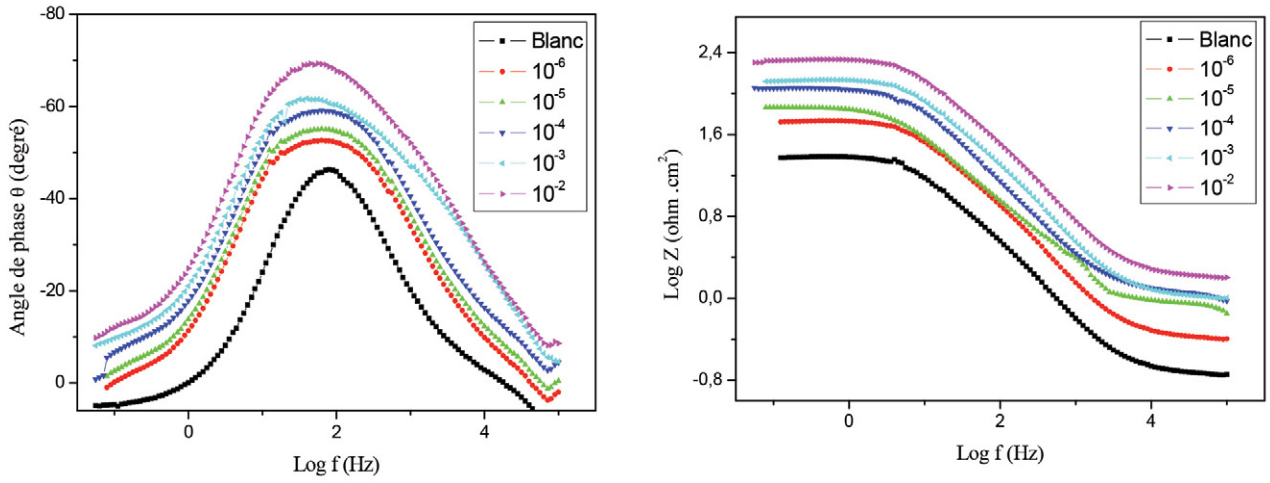

Figure 5. Phase angle and the Bode diagram for different concentrations of the compound L in HCl at 25 °C.

varying amounts of compound L. The Nyquist spectra are presented as a single capacitive loop, confirming that the corrosion of carbon steel in acidic media in the presence and absence of inhibitor is mainly controlled by the charge transfer process.[61] All of the Nyquist plots are semi-circular and their diameters are affected by changes in inhibitor concentration. This indicates a more extensive coverage of the compound on the surface of the carbon steel, suggesting greater inhibition.[25] The resulting semicircles can be observed on the real Z of the Nyquist plot. This is often due to frequency dispersion caused by the roughness of the metal surface [62]. In the Bode plots (Figs. 5 & 6), it can be seen that the log (Z) values increased for different inhibitor concentrations, parallel to the decrease in the frequency values; this can be attributed to the formation of a protective layer on the surface of the carbon steel. On the other hand, the phase angle values increase up to a more negative value of 70° for an optimal concentration of 10^{-2} M compared to the blank (45°) which implies that the tested inhibitor is effective. The equivalent circuit representing the carbon steel/solution interface, without (a) and with (b) inhibitor, is shown in Fig. 7. This circuit consists of the electrolytic resistance (R_s), the charge transfer resistance (R_{ct}), and the constant phase element (CPE). The double layer capacitance (C_{dl}) allows a more accurate correction of the experimental results.[63] The use of a constant phase element (CPE) instead of a regular capacitor is recommended to represent the frequency dispersion caused by surface heterogeneity due to corrosion in an acidic environment. The capacitive response of corrosion product films is represented by C_f. The parameter 'CPE' is usually referred to as the prefactor of a constant phase element (CPE), CPE does not specify a value for the capacitance. It has to be calculated according to the following equation: $Cx=[(RxQx)1nx/]\ Rx/$ where 'x' represents the number for each RC- loop in the EEC (x =1,2 …).

As the inhibitor concentration increases, the thickness (e) of the double layer capacitance increases. Increasing the concentration of the inhibitor decreases C_{dl}. This decrease in C_{dl}, which can result from a decrease in the local dielectric constant ((ε) and/or an increase in the thickness (e) of the electric double layer, suggested that the inhibitors function by adsorption at the metal/solution interface. This can be verified according to the formula in the Helmholtz model[64]:

$$C_{dl} = \frac{\varepsilon_o \varepsilon}{e} \tag{12}$$

where (ε_o) is the relative dielectric constant.

The use of a constant phase element (CPE) instead of a regular capacitor is recommended to represent the frequency dispersion caused by surface heterogeneity due to corrosion in an acidic environment.

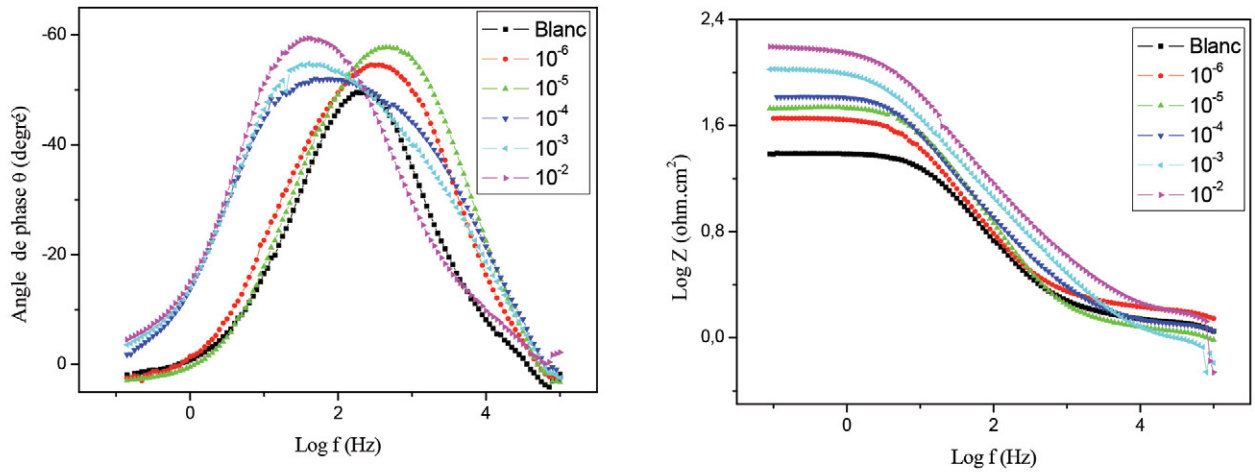

Figure 6. Phase angle and the Bode diagram for different concentrations of the compound L in H_2SO_4 at 25 °C.

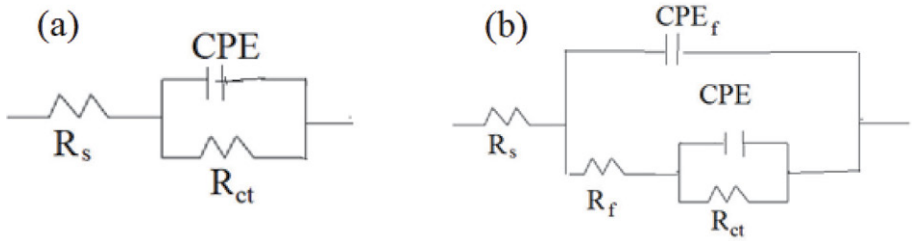

Figure 7. Equivalent circuit diagram (a) is used to fit carbon steel in blank solution, and (b) is used to fit carbon steel in solution containing L (R_f is a film resistance).

The R_{ct} values are determined by analyzing the impedance difference between high and low frequencies along the real axis, as suggested by Tsuru and Haruyama.[65,66] The C_{dl} values are determined using the equation (13):

$$C_{dl} = \frac{1}{2\pi\,\omega_{max}} \times \frac{1}{Rct} \quad (13)$$

Where, C_{dl}: double layer capacitance; R_{ct}: charge transfer resistance; and ω_{max}: high frequency. The corrosion inhibition efficiency of carbon steel is determined by the charge transfer resistance using the equation (14) [67]:

$$\eta_z(\%) = \frac{Rct_i - Rct_0}{Rct_i} \times 100 \quad (14)$$

R_{ct0} and R_{cti} values of the charge transfer resistances of the carbon steel after immersion in HCl and H_2SO_4 in the absence and presence of inhibitors L, respectively.

EIS was used to evaluate the electrochemical characteristics and inhibition efficacy of inhibitor L at different concentrations for carbon steel corrosion in HCl and H_2SO_4 solutions, as shown in Table 4.

5) It is clear from Fig. 4 that the experimental and theoretical curves are fitted well. The calculated values of chi-square (χ^2) (Table 4) supported the good fitting and the suitable equivalent circuits used.
6) Y_o is the magnitude of the CPE, n is the CPE exponent. The CPE which is considered a surface irregularity of the electrode causes a great depression in Nyquist semicircle diagram, where the metal-solution interface acts as a capacitor with irregular surface. The values of Y_o and n decreases by increasing the concentration of compound L indicating that the adsorption of the compound onto the carbon steel surface is not uniform, so the surface is relatively homogeneous. The adsorption of the compound L on the carbon steel can occurs directly by acceptor-donor interactions between the unbonded electrons of N, the π-electrons and the vacant (d) orbital of the iron.[70]

3. 8. Adsorption Isotherm

The inhibition of metal corrosion by inhibitor L is attributed to adsorption. The corrosion current density,

Table 4. Impedance parameters of carbon steel in HCl and H_2SO_4 at different concentrations of compound L at 25 °C.

Corrosive medium	Concn. (M)	R_s (Ω.cm²)	n	Y_o ($\mu\Omega^{-1}s^n cm^{-2}$) ×10⁻⁶	R_{ct} (Ω.cm²)	C_{dl} (μF/cm⁻²)	θ	η_Z (%)	of Fit² Goodness
HCl	Blank	1.06	0.944	1144	25.1	1128	–	–	18.24×10^{-3}
	10^{-6}	1.49	0.942	542	68.4	520	0.633	63.3	16.47×10^{-3}
	10^{-5}	2.25	0.935	340	78.1	322	0.679	67.9	14.25×10^{-3}
	10^{-4}	1.67	0.931	281	95.7	262	0.738	73.8	15.74×10^{-3}
	10^{-3}	3.51	0.928	253	103.7	229	0.758	75.8	13.57×10^{-3}
	10^{-2}	2.18	0.914	147	153.2	103	0.836	83.6	11.32×10^{-3}
H_2SO_4	Blank	1.12	0.939	722	25.3	705	-	-	15.77×10^{-3}
	10^{-6}	1.32	0.927	589	44.2	568	0.428	42.8	17.22×10^{-3}
	10^{-5}	2.15	0.912	561	52.2	542	0.515	51.5	19.87×10^{-3}
	10^{-4}	2.44	0.911	457	70.2	445	0.640	64.0	18.24×10^{-3}
	10^{-3}	1.65	0.907	377	110.5	358	0.771	77.1	16.24×10^{-3}
	10^{-2}	1.65	0.901	216	163.6	208	0.845	84.5	18.55×10^{-3}

These results allow us to conclude that:

1) The η_z increases with increasing the concentration of inhibitor L, confirming that this compound has an inhibiting power for the carbon steel in HCl and H_2SO_4.
2) The double layer formed at the electrode-solution interface acts as an electrical capacitor. Its capacitance (C_{dl}) decreases as water molecules are replaced by inhibitor molecules that adsorb onto the steel surface, forming a protective layer.
3) As the inhibitor concentration increases, the thickness of the adsorbed layer increases i.e. R_{ct} increases. This finding is consistent with existing research on steel corrosion inhibition.[68,69]
4) Inhibition efficiencies reported by gravimetric, electrochemical impedance spectroscopy and Tafel polarization are in agreement.

transfer resistance and corrosion rate of the inhibited steel are proportional to the ratio of the area covered by the inhibitor (θ = η (%)/100). Different types of isotherms were tested to identify the appropriate type of adsorption corresponding to this inhibitor: Langmuir, Temkin and Frumkin. The Langmuir isotherm given by equation (15) was found to be the most appropriate:[71,72]

$$\frac{C_{inh}}{\theta} = \frac{1}{K_{ads}} + C_{inh} \quad (15)$$

C_{inh}: inhibitor concentration, K_{ads}: adsorption equilibrium constant, and θ: surface coverage expressed by the ratio η /100.

The variation of the $\frac{C_{inh}}{\theta}$ ratio as a function of C_{inh} is linear for the three methods of gravimetric, EIS, and Tafel curves at 25 °C (Fig. 8). These results indicate that the ad-

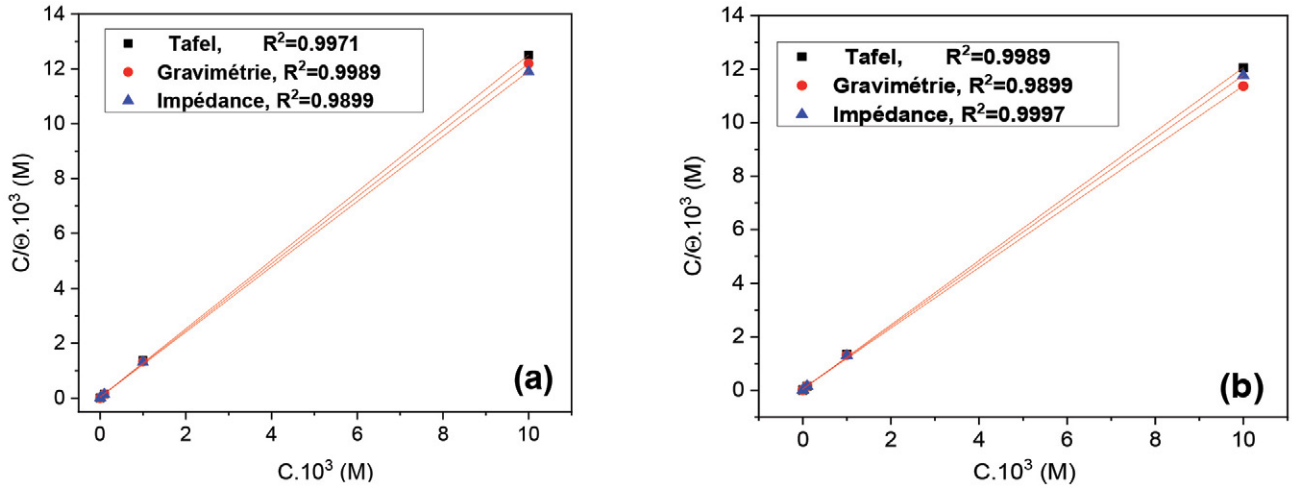

Figure 8. Langmuir adsorption isotherms for carbon steel in HCl (a) and H_2SO_4 (b) in the presence of compound L for all three methods.

sorption of inhibitor L on carbon steel in HCl and H_2SO_4 media is represented by Langmuir adsorption isotherm, with linear correlation coefficients ($R^2 = 0.9999$) close to 1 and all slope values close to unity.[73]

The values of K_{ads} (Adsorption constant) were determined from the intersection with the $\frac{C_{inh}}{\theta}$ / axis (Fig. 8). Equation (16) relates the K_{ads} constant to the standard free adsorption energy (ΔG°_{ads}).[74]

$$K_{ads} = \frac{1}{55{,}55} \exp\left(\frac{-\Delta G^{\circ}_{ads}}{RT}\right) \quad (16)$$

R: ideal gas constant (8.314 J mol^{-1} K^{-1}); T: temperature (K). The value 55.55 is the concentration of water in solution (mol. L^{-1}).

Table 5 shows the values of K_{ads} and ΔG°_{ads} obtained from the Langmuir isotherm.

Table 5. Thermodynamic parameters for compound L adsorbed on carbon steel in HCl and H_2SO_4 at 25 °C for all three methods

Methods	Medium	R^2	$K_{ads}.10^{-4}$ (M^{-1})	$-\Delta G^{\circ}_{ads}$ (kJ mol^{-1})
Gravimetric	1 M HCl	0.9985	2.99	35.48
	0.5 M H_2SO_4	0.9997	2.90	35.41
Tafel	1 M HCl	0.9999	3.09	35.57
	0.5 M H_2SO_4	0.9998	2.80	35.32
EIS	1 M HCl	0.9998	2.93	35.43
	0.5 M H_2SO_4	0.9999	2.90	35.41

The values of the adsorption constant K_{ads} are more significant in the H_2SO_4 medium than in the HCl medium: the compound L is adsorbed faster on the active sites of the steel in H_2SO_4 solution than in the HCl solution.[75] Furthermore, the negative values of ΔG°_{ads} and the high values of K_{ads} reflect the spontaneity of the adsorption process and the strength of the adsorption layer on the steel.[76] Generally, values of ΔG°_{ads} close to –20 kJ mol^{-1} or lower energies are associated with interactions between charged molecules and metal charges through physisorption. On the other hand, those close to –40 kJ mol^{-1} or higher involve a charge transfer between the inhibitor molecules and the metal surface through the formation of covalent or coordination bonds (chemisorption).[76] The values of ΔG°_{ads} of the inhibitor L on the steel in the medium of HCl and H_2SO_4 are between –35 and –40 kJ mol^{-1} (Table 5); this compound L is demonstrated to undergo physisorption and chemisorption on the steel surface.[77,78]

3. 9. Effect of Temperature

Temperature can affect how a chemical behaves in a corrosive environment. It can alter the interaction between steel and inhibitor in a certain environment. Rising temperature speeds up corrosion reactions and can reduce the corrosion resistance of steel. We conducted a potentiodynamic study with and without compound L at different concentrations and temperatures. The values of i_{corr}, E_{corr}, and η_p of compound L versus temperature are shown in Table 6.

These results confirm that this inhibitor is almost stable for temperatures between 25 and 55 °C. The η_p of the compound L decreases slightly with the increase of the temperature T. This indicates the stronger adsorption binding of compound L to the surface. It can be concluded that chemisorption is present in addition to physisorption. The evolution of the corrosion currents in the corrosive media (HCl and H_2SO_4) without compound L shows an increase in the metallic dissolution with the increase in temperature T. The increase of the current density with the temperature at a constant concentration of the inhibitor is lower than in the absence of the inhibitor.

These results confirm that compound L inhibits corrosion at different temperatures, suggesting physical and

Table 6. Variation of temperature on the electrochemical properties of carbon steel in HCl and H_2SO_4 with different concentrations of compound L

Acid Solutions		1M HCl			0.5 M H_2SO_4		
Temp. (°C)	C_{Inh} (M)	E_{corr} (mV/SCE)	i_{corr} (mA cm^{-2})	η_p (%)	E_{corr} (mV/SCE)	i_{corr} (mA cm^{-2})	η_p (%)
25	00	547.2	0.60	-	557.2	0.70	-
	10^{-6}	523.0	0.24	60.1	534.0	0.44	37.14
	10^{-5}	520.9	0.21	65.2	539.2	0.31	55.71
	10^{-4}	519.8	0.19	68.33	538.7	0.24	65.71
	10^{-3}	518.0	0.16	73.33	511.1	0.18	74.28
	10^{-2}	508.9	0.12	80.2	527.0	0.12	82.85
35	00	552.5	1.45	-	559.7	1.06	-
	10^{-6}	551.3	0.57	60.3	555.7	0.79	25.47
	10^{-5}	547.2	0.50	65.51	555.8	0.57	47.16
	10^{-4}	542,2	0.46	68.27	548,0	0,42	61,32
	10^{-3}	561.2	0.40	72.41	559.4	0.33	69.81
	10^{-2}	556.2	0.29	80.2	561.8	0.22	80.01
45	00	561.8	1.79	-	565.8	3.06	-
	10^{-6}	565.8	0.96	46.36	554.1	2.39	21.89
	10^{-5}	547.1	0.78	56.42	559.1	1.84	39.86
	10^{-4}	544.8	0.60	66.48	564.3	1.14	62.74
	10^{-3}	548.8	0.51	71.50	555.9	0.82	73.20
	10^{-2}	538.6	0.41	77.09	559.1	0.70	77.12
55	00	529.0	3.55	-	559.6	4.93	-
	10^{-6}	544.0	2.67	24.78	567.8	4.20	14.80
	10^{-5}	563.0	1.72	51.54	559.2	3.94	20.08
	10^{-4}	565.4	1.43	59.71	555.2	2.14	56.59
	10^{-3}	575.0	1.09	69.29	564.0	1.79	63.69
	10^{-2}	593.8	0.90	74.64	647.5	1.23	75.25

chemical adsorption.[79] Indeed, the decrease in inhibitor efficacy with temperature was explained by Van der Waals type physical interactions between the steel surface and the inhibitor.[80] These interactions are sensitive to thermal agitation and are easily disrupted as the temperature increases. As the temperature increases, the balance between adsorption and desorption shifts towards desorption, reducing the inhibitory effect of the compound..[17]

Fig. 9 shows the variation of the logarithm of the corrosion current density as a function of the reciprocal temperature. The activation energies calculated from the Arrhenius relationship in Table 7 for different inhibitor concentrations in HCl and H_2SO_4 are determined by linear regression (Fig. 9).

3. 9. 1. Determination of Activation Parameters

Many authors[81,82] have used the Arrhenius equation to study the effect of temperature (T) on the corrosion current density in an acidic environment, showing that the logarithm of the corrosion current density (i_{corr}) is linearly correlated with T^{-1}. The activation parameters of the corrosion process were determined at different temperatures, both with and without inhibitor L. The activation energy (E_a) was calculated utilizing the Arrhenius equation (16).[83]

$$i_{corr} = A\exp(\frac{-E_a}{RT}) \quad (16)$$

where $E_{a:}$ the activation energy and A: the pre-exponential factor.[83]

These results show an increase in activation energies for the different inhibitor concentrations compared with HCl and H_2SO_4 without inhibitor. According to Radovic's theory, a classification of inhibitors is based on the comparison of the activation energies obtained without inhibitor (E_a) and with inhibitor (E_{ai}). When $E_{ai} > E_a$, the inhibitors are adsorbed on the substrate by bonds of an electrostatic nature (weak bonds).

This type of bond is temperature sensitive and will not provide effective corrosion control as the temperature increases. Generally, the temperature affects the corrosion phenomena. The inhibitor is physically adsorbed at low temperatures, while chemisorption is favored at high temperatures. As temperature increases, the increase in activation energy results from a decrease in inhibitor adsorption

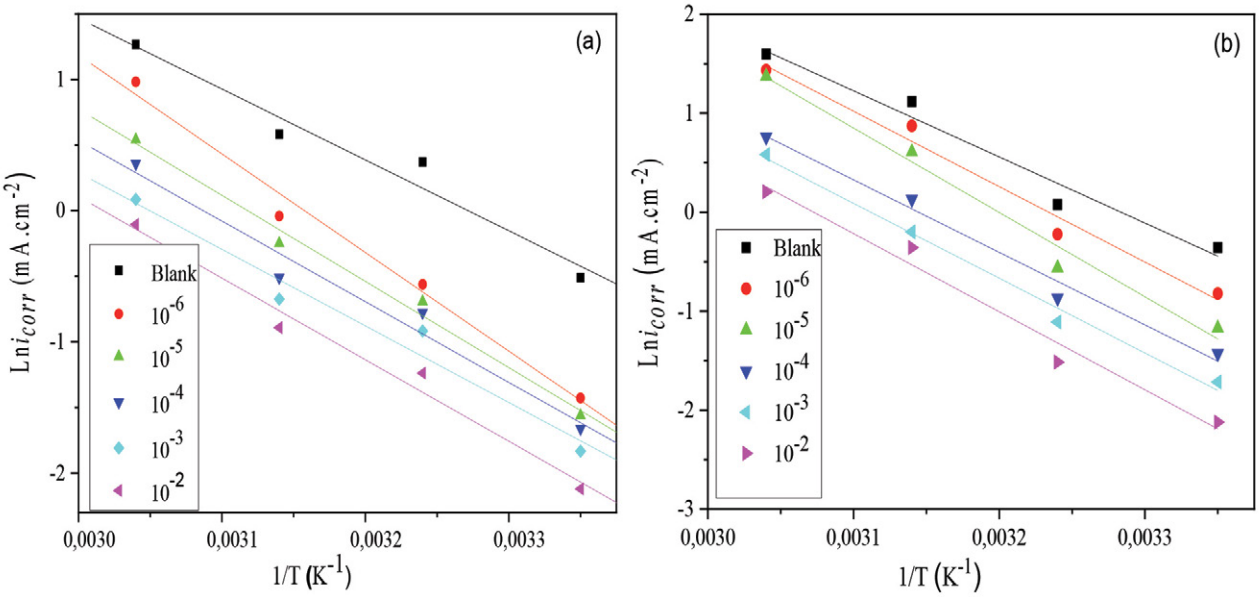

Figure 9. Arrhenius plots for carbon steel in HCl (a) and H_2SO_4 (b) solutions with different concentrations of compound L

on the steel surface.[84,85] This behavior is attributed to the physisorption of the inhibitor on the metal surface.[86] The corrosion of steel in the presence of an inhibitor is influenced by the reaction taking place on the bare steel surface and the diffusion of Fe^{2+} ions through the inhibitor layer. Let us recall the formula of the Arrhenius equation, which determines the activation of enthalpy and the activation of entropy:

$$i_{corr} = \frac{RT}{Nh} \exp\left(\frac{\Delta S^{\circ}_a}{R}\right) \exp\left(-\frac{\Delta H^{\circ}_a}{RT}\right) \quad (17)$$

where: *h*: Planck's constant, *N*: Avogadro's number, ΔH°_a: enthalpy of activation, and ΔS°_a: entropy of activation.

The variation of $\mathrm{Ln}\left(\frac{i_{corr}}{T}\right)$ as a function of $\frac{1}{T}$ is a straight line with slope $\left(-\frac{\Delta H^{\circ}_a}{R}\right)$ and y-intercept equal to $\left(\mathrm{Ln}\left(\frac{R}{Nh}\right) + \frac{\Delta S^{\circ}_a}{R}\right)$ (Fig. 10). The values of enthalpies ΔH°_a and entropies ΔS°_a in HCl and H_2SO_4 are given in Table 7.

The values of the enthalpy (ΔH°_a) show the endothermic nature of the dissolution process of the carbon steel. The increase in enthalpy with increasing concentration reflects a decrease in the dissolution of the metal. The negative entropy (ΔS°_a) values indicate that the activated complex represents an associating step rather than a dissociating step, meaning that a decrease in disorganization occurs from the reactants to the activated complex.[87]

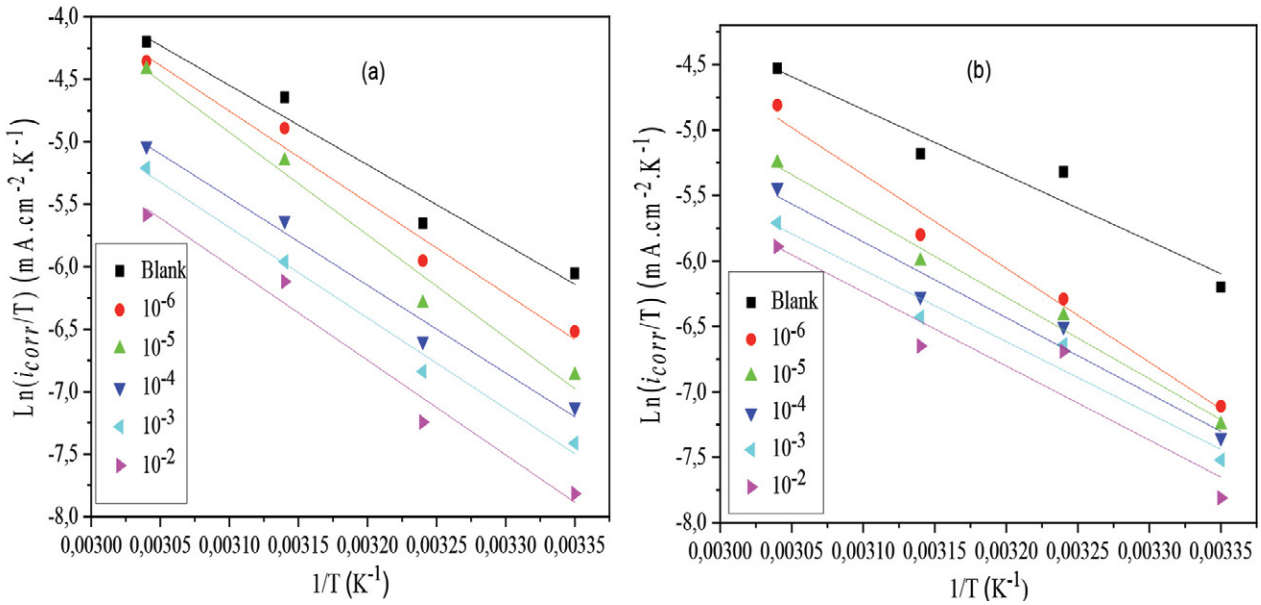

Figure 10. Arrhenius plots for carbon steel in HCl (a) and H_2SO_4 (b) solutions at different concentrations of the compound.

Table 7. Thermodynamic characteristics of carbon steel in HCl and H_2SO_4 at different concentrations of the compound L.

Acid Solutions	Concentration (M)	E_a (kJ mol^{-1})	ΔH°_a (kJ mol^{-1})	$-\Delta S^\circ_a$ (J mol^{-1} K^{-1})
1 M HCl	Blank	44.90	41.76	109.32
	10^{-6}	62.55	59.65	58.01
	10^{-5}	54.61	51.91	84.53
	10^{-4}	51.12	48.21	97.67
	10^{-3}	48.58	45.63	106.32
	10^{-2}	51.70	49.05	98.50
0.5 M H_2SO_4	Blank	55.57	52.99	71.58
	10^{-6}	63.40	60.82	49.01
	10^{-5}	70.89	68.31	27.20
	10^{-4}	60.95	58.37	62.36
	10^{-3}	62.87	60.29	58.40
	10^{-2}	65.63	63.05	52.39

Table 8. Thermodynamic parameters for compound L adsorbed on carbon steel in HCl and H_2SO_4 at 25–55 °C

Acid solutions	T (°C)	R^2	$K_{ads}.10^{-4}$ (M^{-1})	$-\Delta G^\circ_{ads}$ (kJ mol^{-1})
1 M HCl	25	0.9999	3.09	35.57
	35	0.9992	2.71	35.24
	45	0.9988	3.27	35.71
	55	0.9994	2.69	35.22
0.5 M H_2SO_4	25	0.9979	2.81	35.33
	35	0.9956	1.22	33.26
	45	0.9963	2.30	34.83
	55	0.9962	1.77	34.18

3. 9. 2. Adsorption Isotherms at Various Temperatures

To compare the ΔG°_{ads} of the different temperatures studied at different concentrations of compound L from the Tafel curves, we plotted $\left(\frac{c}{\theta}\right)$ as a function of C of compound L (Fig. 11).

The plot of $\left(\frac{c}{\theta}\right)$ versus the concentration C is linear (Fig. 11), confirming that the adsorption of the compound (L) occurs according to the Langmuir isotherm model with a correlation of unity. The thermodynamic quantities K_{ads} and ΔG°_{ads} obtained from the adsorption isotherm under the same conditions mentioned above are regrouped together in the Table 8.

The ΔG°_{ads} values reflect the spontaneity of the adsorption process and the stability of the adsorbed layer on the steel surface.[88] The calculated values of ΔG°_{ads} are between –33 and –36 kJ mol^{-1}, showing that inhibitor L can be defined as physisorption and chemisorption on the steel surface[89] (Table 8). The values of ΔG°_{ads} decrease with T (become more negative), so the adsorption process is endothermic.[90] In conclusion, the inhibition power decreases significantly at high temperature, but the activation energy increases in the presence of the compound.[91,92] The adsorption mode can be considered as physical and chemical adsorption.[87]

3. 10. Surface Examination

3. 10. 1. SEM Analysis

To complete and confirm the corrosion inhibition results, we used scanning electron microscopy (SEM). SEM images of carbon steel after immersion for 6 h in HCl and H_2SO_4 without and with compound L at an optimum concentration of 10^{-2} M are shown in Fig. 12. SEM observations were made on steel samples before immersion (steel alone (a)) and after immersion for 6 h in HCl (b), H_2SO_4 (c), HCl + L 10^{-2} M (d) and H_2SO_4 + L 10^{-2} M (e). By comparing the

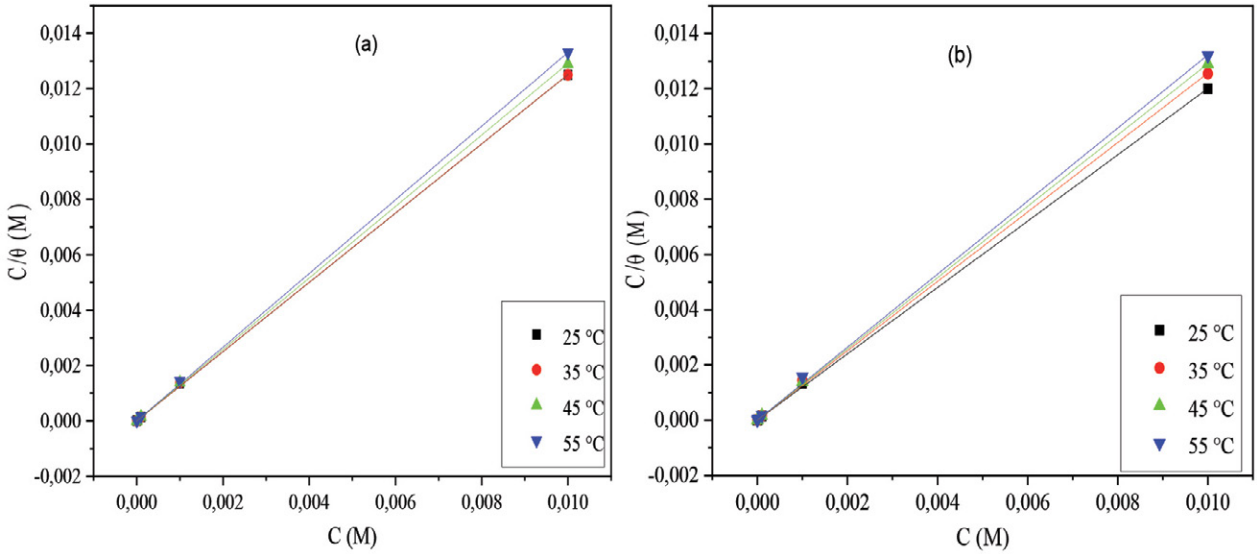

Figure 11. Model of the Langmuir adsorption isotherm of carbon steel in HCl (a) and H_2SO_4 (b) at different concentrations of L for T = 25, 35, 45 and 55 °C.

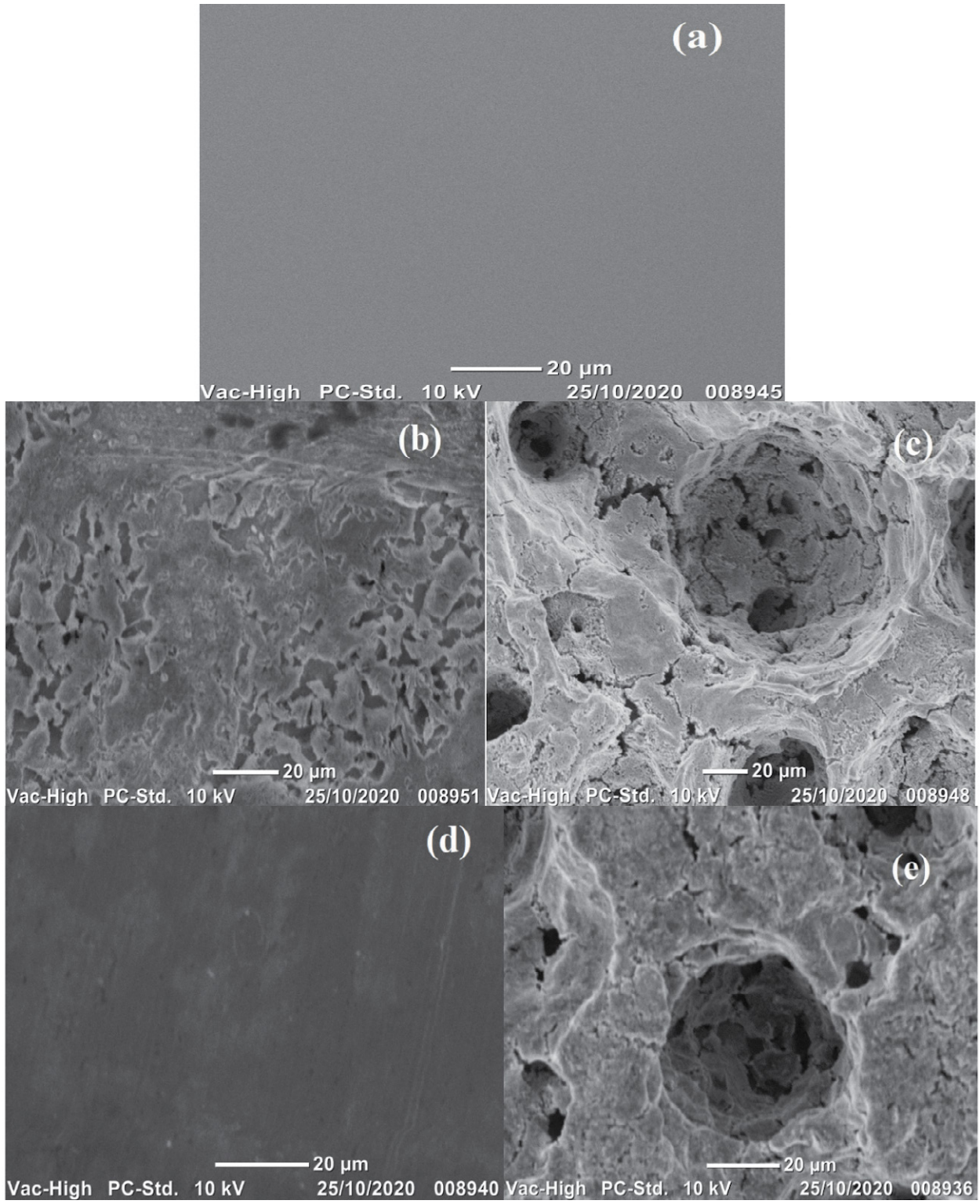

Figure 12. SEM micrographs of the carbon steel surface after immersion for 6 h: (a) bare, (b) in 1.0 M HCl alone (c) in 0.5 M H_2SO_4 alone, (d) treated with L 10^{-2} M in HCl, (e) treated with L 10^{-2} M in H_2SO_4.

surface finish between the untreated samples (Fig. 12a) and the treated samples (Fig. 12b, c, d, e). As shown in Fig. 12b, c in the absence of an inhibitor L, the surface is severely damaged with many pits and cavities, confirming that the steel is dissolving in the aggressive medium. Sulfuric acid (H_2SO_4) reacts aggressively with crevice corrosion[83] compared to HCl, which attacks steel by pitting. This is confirmed by the mass loss (Table 2) and the SEM image. In the

presence of an inhibitor, the morphology of the HCl deposits is different from that of the H_2SO_4 deposits (Fig. 12d, e). Fig. 12e shows a slight decrease compared to Fig. 12c, on the other hand, Fig. 12d shows an excellent inhibition compared to Fig. 12b due to the addition of L, which forms a protective film against corrosion adsorbed on the surface.[47] It is discovered that the steel is much less attacked in the presence of L, confirming the inhibition that occurs at the metal surface. This surface treatment is credited with creating a protective coating or reducing the rate of corrosion on the steel surface.[93]

3. 10. 2. Atomic Force Microscopy (AFM) Analysis

AFM photos with three dimensional are a significant examination for determining the metal surface roughness at highest resolution in nanometer fraction. An AFM analysis was conducted on the carbon steel surface to check the existence of an inhibitor film.[94] AFM images and force curves are shown in Fig. 13. Fig. 13a shows free carbon steel, Fig. 13b, c display metal after 6 hours of exposure in 1.0 M HCl and 0.5 M H_2SO_4 solutions, respectively. Fig. 13d treated with L 10^{-2} M in HCl, and Fig. 13e treated with L 10^{-2} M in H_2SO_4. The mean roughness value of the carbon steel surface that was exposed to a 1.0 M HCl and 0.5 M H_2SO_4 solution but was not treated with the inhibitor was substantially greater at 320 nm and 390 nm respectively. The corrosive effects of the acid over the course of the 6 hour rust test period left the carbon steel surface with a porous structure and deep fractures, which led to this heightened roughness. However, when the tested inhibitors are applied at the optimum concentration (10^{-2} M),

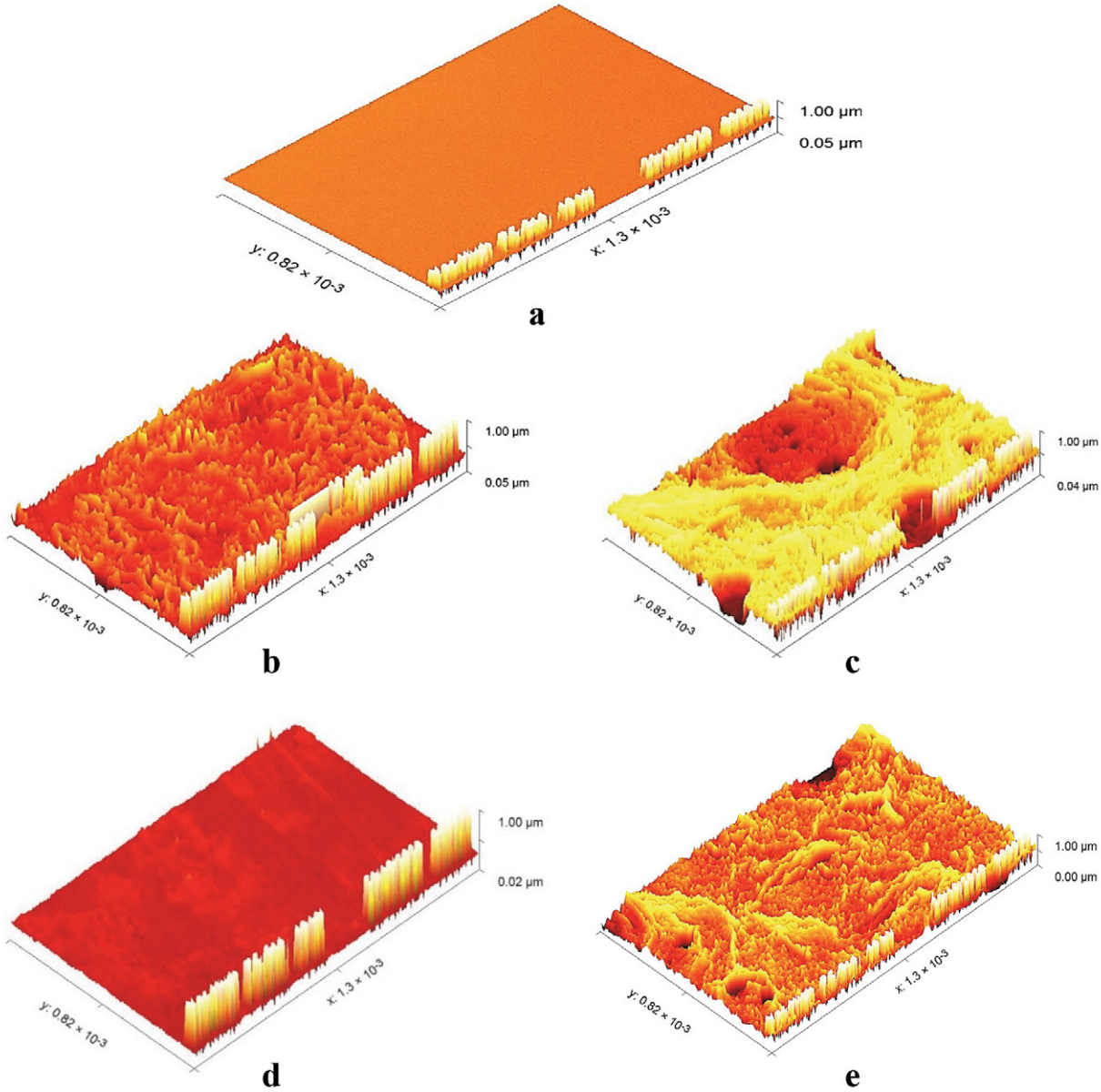

Figure 13. AFM micrographs of the carbon steel surface after immersion for 6 h: (a) bare, (b) in 1.0 M HCl alone (c) in 0.5 M H_2SO_4 alone, (d) treated with L 10^{-2} M in HCl, (e) treated with L 10^{-2} M in H_2SO_4.

the average roughness for 10^{-2} M dissolved in HCl & 10^{-2} M treated with H_2SO_4 is reduced to 90 & 120 nm, respectively. The test inhibitor effectively maintains the hardness of the carbon steel as indicated by the drop in the roughness value.[95]

3. 11. Theoretical Studies

3. 11. 1. Quantum Chemical Study and Mechanism of Inhibition Action

DFT is used to confirm the experimental results obtained. Electronic properties and quantum chemical calculations were used to evaluate how the molecular structure affects the inhibitory efficacy of compound L. The optimized structure and molecular density distributions of the boundary orbitals (HOMO and LUMO) of compound L are determined by the B3LYP/6-31G (d, p) method, as illustrated in Fig. 14.

Eqs. 1 to 7 were used to calculate these quantum chemical parameters (E_{HOMO}, E_{LUMO}, ΔE_{gap}, dipole moment (μ), absolute electronegativity (χ), absolute hardness (η), softness (σ), electrophilicity index (ω), and fraction of electrons transferred (ΔN)[96] for the estimated structure of compound L in the gas and aqueous phases (Table 9).

E_{HOMO}, E_{LUMO}, and ΔE_{gap} are consistent with the inhibition efficiency.[97] In all cases, decreasing $\Delta Egap$ and E_{LUMO} and increasing E_{HOMO} indicate high inhibition efficacy.[96] If the value of ΔE_{gap} is not high, then the electrons taken from the HOMO do not require much energy. This is in agreement with the experimental results and the calculated values of ΔN.[97] An inhibitor L can either take electrons from the d-orbital of the metal or contribute an electron to the vacant d-orbital of the metal ion, forming a covalent bond. Therefore, the formation of the latter depends on the value of E_{LUMO}. The low value of E_{LUMO} = -0.45 eV indicates that it is easy to receive electrons from the d-orbital of a metal.[98,99] The parameter ΔE_{gap} affects the adsorption ability of the inhibitor molecule on the steel surface. The results show that our inhibitor L has a low ΔE_{gap} value of 4.4 eV, confirming its reactivity with metal atoms.[100] The inhibitory potential of a molecule is related to its dipole moment (μ).[101] As μ increases, so does adsorption. The phenomenon is a quasi-substitution process in which the inhibitor molecule in the aqueous phase replaces water molecules on the carbon steel zone, causing water molecules to desorb onto the steel. The value of μ_{inb}

Table 9. Calculations obtained for the compound L in the gas phase and in the aqueous phase using the DFT method.

Quantum parameters	Gas phase	Aqueous phase
E_{tot} (eV)	–32343	–32343.47
E_{HOMO} (eV)	–4.85	–4.4
E_{LUMO} (eV)	–0.45	–1.2
$\Delta Egap$(eV)	4.4	3.2
μ (Debye)	5.7	6.11
ΔN(eV)	2.2	1.6
σ (eV^{-1})	0.45	0.62
χ (eV)	2.65	2.8
ω (eV)	1.6	2.46
ΔN	0.98	1.31

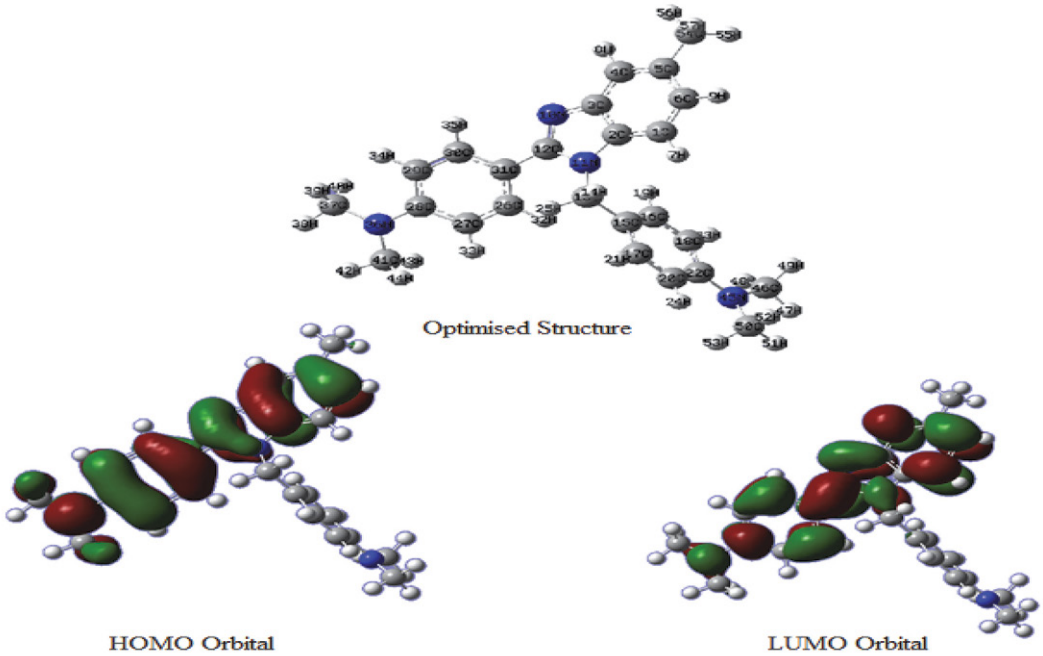

Figure 14. Optimum structure and density distribution of the frontier molecular orbitals (HOMO and LUMO) of compound L obtained by the B3LYP/6-31(d.p) method.

(5.7 Debye) is higher than that of μ_{H2O} (1.88 Debye). The observed low energy difference observed and the high value of the dipole moment lead to the transfer of electrons from the molecule to the surface. This phenomenon occurs during the adsorption process on the surface of carbon steel.

Molecular stability and reactivity depend on the absolute hardness and softness of the molecules. A hard molecule is characterized by a significant energy difference, while a soft molecule is characterized by a low energy difference. Hard molecules have reduced reactivity compared to soft molecules due to their limited ability to donate electrons to an acceptor. The adsorbate could be situated in the region of the molecule with the highest σ value.[100] Inhibition efficiency is high, with an overall hardness value of 2.2 eV and an overall softness value of 0.45 eV^{-1} (Table 9). These results are in agreement with those reported in the literature.[101,102]

The small energy difference indicates that the inhibitor molecule is reactive with the metal atoms. The electrophilicity index (ω) of compound L is 1.6 eV, indicating a high inhibition value.[103] According to Lukovits,[104] as the electron transport capacity to the metal surface increases, so does the inhibition. As the strength of the inhibitory iron link increases (due to the increase in ΔN), the level of corrosion inhibition through chemisorption also increases. The results indicate that the inhibitor L has good inhibition efficiency due to its low electrophilicity (ω = 1.6 eV) and high fraction of electrons transmitted value ($\Delta N = 0.98$). The inhibitor tested in this study had a ΔN value of less than 3.6 (Table 9).[105,106] Confirmation that the inhibitor can contribute electrons to iron to form coordinated links, leading to the formation of an inhibition layer that prevents corrosion. The electronegativity value of (χ) L was 2.65 eV, which is lower than the electronegativity of Fe (χ = 7 eV). This suggests that there was electron transfer from the highest occupied molecular orbital (HOMO) of the inhibitor to the vacant 3d orbital of Fe. The electron transfer from the filled Fe 4s orbital to the lowest unoccupied molecular orbital (LUMO) of the inhibitor is greater. The electron flow from the benzimidazole substituted molecule results in greater inhibition efficiency.[76]

The molecular electrostatic potential (MEP) is related to electron density and is a valuable tool for identifying the locations of electrophilic and nucleophilic reaction sites.[107] We used the optimized geometry of compound L. The nucleophilic active region is indicated by light blue and blue colors on the MEP map. The electrophilic active region is shown in red and yellow. In the MEP contours, the yellow and red lines indicate the positively and negatively charged regions, respectively. Fig. 15 shows that regions of increased electron density are located between the heteroatoms and the conjugated double bonds. The electrophilic sites of the molecule are located in the center around the nitrogen atoms (N10, N11, and N36). In this way, the nitrogen atoms induce nucleophilic reactions to limit corrosion.[103]

Compound L can form chelate species on the carbon steel surface by transferring electrons between the benzimidazole groups and the iron (d-orbital), resulting in a coordinated covalent bond by chemical adsorption. The carbon steel acts as an electrophile, attracting the negatively charged sites of compound L. The compound has nucleophilic centers that serve as adsorption sites, such as heteroatoms with free electron pairs, electronegative functional groups, and double electrons.[108] The adsorption of the inhibitor is controlled by the transfer of electrons from the most highly occupied molecular orbital (HOMO) of the inhibitor to the empty d-orbital of the metal. The HOMO energy level of the molecule is mainly located on the planar group of the benzimidazole and the phenyl substituent N (CH_3).

The results indicate that the molecule under study has low spatial energy. This proves the high reactivity as well as the high inhibitory efficacy of compound L. This is in agreement with the experimental studies. Electronic properties alone are insufficient to predict the protective performance of a compound under investigation, although they are successful in exploring the mechanism of action of the inhibitor.

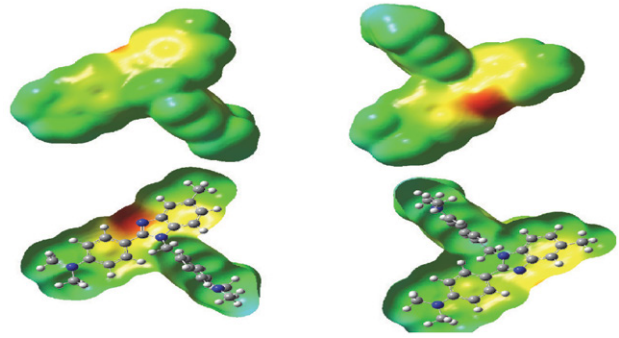

Figure 15. MEP map and counter plot of compound L.

3. 11. 2. Simulations of the Molecular Dynamics of the [L/Fe (1 1 0)]

Therefore, careful modeling of the direct interaction of the inhibitor with carbon steel is essential. Molecular dynamics simulations were used to study the interaction between compound L and the Fe (1 1 0) surface. This was done to gain additional information about the adsorption process of this chemical on the metal surface.

The side (a) and top (b) views of the low energy configuration for the adsorption of compound L on the Fe (1 1 0) surface obtained from simulations are shown in Fig. 16. Our compound is preferentially oriented parallel to the Fe (1 1 0) surface, which increases the surface coverage.[109] From Fig. 16, we can see that L is adsorbed parallel to the iron surface and could be chemically bound. The adsorp-

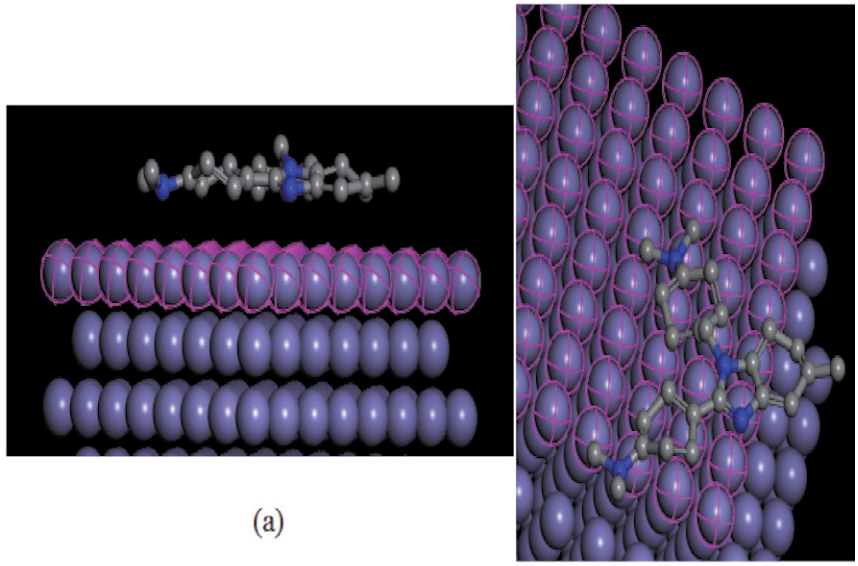

Figure 16. Equilibrium adsorption configurations of compound L on surface Fe (1 1 0) (a) side view, (b) top view

tion mechanism is due to the fact that the π-electrons of the aromatic ring and the free nitrogen electrons in the molecule occupy the empty d-orbitals of the Fe and form a protective film on the surface of the metal.

According to our results, the average centroid distance (d) between the benzimidazole derivative L and the surface of Fe (1 1 0) is about 2.9 Å, which is slightly larger than the sum of the covalent rays (about 2 Å) of N and of the Fe atom. The reactivity of Fe (1 1 0) seems to be at the beginning of the dipole-dipole interaction, which gives a very stable parallel adsorption structure and a mode of apparent chemisorption + physisorption.[110]

4. Conclusion

This study reports the preparation and characterization of a novel benzimidazole compound, 4-(1-(4-(dimethylamino)benzyl)-5-methyl-1H-benzo[d]imidazol-2-yl)-N,N-dimethylaniline (L) by 1H NMR, UV-vis, and FT-IR. It was also investigated how well this chemical performed in reducing the corrosion rate of carbon steel in solutions containing 1 M HCl and 0.5 M H_2SO_4 at various exposure concentrations and temperatures.

One can draw the following conclusions:

1. The use of compound L as a corrosion inhibitor has shown that this inhibitor is effective against the corrosion of carbon steel in HCl and H_2SO_4.
2. Inhibition efficiency increases with increasing concentration of Inhibitor L in all methods used.
3. Analysis of the polarization curves shows that compound L behaves as a mixed-type inhibitor.
4. The adsorption of compound L on carbon steel follows the Langmuir isotherm in both environments. In addition, its adsorption occurs chemically and physically. Electrochemical impedance spectroscopy diagrams are presented as a single capacitive loop.
5. SEM photos of the surface of the compound L show the formation of a protective layer.
6. The results of gravimetric measurements and electrochemical techniques are in concordance.
7. There is a good correlation with increased inhibition efficiency at high values of E_{HOMO}, μ, σ, and ΔN and at lower values of ΔE_{gap}, E_{LUMO}, ω, and η.
8. Theoretical calculations agree well with experimental methods, demonstrating the importance of the molecular structure of this heterocyclic molecule in inhibiting the corrosive process.

5. References

1. N. Insyirah Hairul Salleh, A. Abdullah, *J. Chem.* **2019**, *19*, 747–752. **DOI:**10.22146/ijc.39707
2. D. K. Lavanya, F. V. Priya, D. P. Vijaya, *J. Fail. Anal. Prev*. **2020**, *20,* 494–502. **DOI:**10.1007/s11668-020-00850-9
3. H. Lgaza, S. K. R. Saha, A. Chaouiki, K. Subrahmanya Bhat, R. Salghi Shubhalaxmi, P. Banerjee, I. H. Ali, M. I. Khan, F. I. Min Chung, *Constr. Build. Mater*. **2020**, *233,* 117320–117333. **DOI:**10.1016/j.conbuildmat.2019.117320
4. H. Jwad Habeeb, H. Mohammed Luaibi, R. Mohammed Dakhil, A. Amir, H. Kadhum Ahmed, T. S. Gaaz Al-Amiery, *Respir. Physiol.* **2018**, *8,* 1260–1267. **DOI:**10.1016/j.rinp.2018.02.015
5. M. F. L. P. Carlos, A. Valbon, M. A. Neves, M. R. L. Santosa, *J. Braz. Chem. Soc.* **2018**, *29*, 2542–2553. **DOI:**10.21577/0103-5053. 20180133.
6. H. Schiff, *Ann. Chem.* **1864**, *131*, 118–119.

DOI:10.1002/jlac.18641310113
7. S. Belaid, A. Landreau, S. Debbar, O. Benali- Baitich, G. Bouet, B. Jean-Philippe, *J. Inorg. Bio.* **2008**, *102,* 63–69. **DOI:**10.1016/j.jinorgbio.2007.07.001
8. A. Gennaro, A. A. Isse, F. Maran, *J. Electroanal. Chem.* **2001**, *507*, 124–134. **DOI:**10.1016/S0022-0728(01)00373-4
9. M. G. Hosseini, M. Ehteshamzadeh, T. Shahrabi, *Electrochimica. Acta.* **2007**, *52*, 3680–3685. **DOI:**10.1016/j.electacta.2006.10.041. **DOI:**10.1016/j.electacta.2006.10.041
10. H. Keleş, M. Keleş, I. Dehri, O. Serindag, *Mater. Chemi. Phys.* **2008**, *112,* 173–179. **DOI:**10.1016/j.matchemphys.2008.05.027
11. E. E. Elemike, H. U. Nwankwo, D. C. Onwudiwe, E. C. Hosten, *J. Mol. Struct.* **2017**, *1147,* 252–265. **DOI:**10.1016/j.molstruc.2017.06.104. **DOI:**10.1016/j.molstruc.2017.06.104
12. G. Schmitt, B. Olbertz, *Werk. Korros.* **1978**, *29,* 451–456. **DOI:**10.1002/maco.19780290704
13. E. AltunbaşŞahin, F. Tezcan, R. Solmaz, G. Kardaş, *J. Adhes. Sci. Technol*. **2019**, 1-18. **DOI:**10.1080/01694243.2019.1662202
14. A. Keleşoğlu, R. Yıldız, I. Dehria, *J. Adhes. Sci. Technol.* **2019**, *33,* 2010–2030. **DOI:**10.1080/01694243.2019.1623967
15. M. Hosseini, S. F. L. Mertens, M. Ghorbani, M. R. Arshadi, *J. Mater. Chem. Phys.* 2003, *78,* 800–808. **DOI:**10.1016/S0254-0584(02)00390-5
16. G. Quartarone, T. Bellomi, A. Zingales, *Corros. Sci.* **2003**, *45,* 715–733. **DOI:**10.1016/S0010-938X(02)00134-8
17. I. B. Obot, N. O. Obi-Egbedi, *Corros. Sci.* **2010**, *52,* 98–204. **DOI:**10.1016/j.corsci.2009.09.002
18. E. SadeghiMeresht, T. ShahrabiFarahani, J. Neshati, *Corros. Sci.* **2012**, *54,* 36–44. **DOI:**10.1016/j.corsci.2011.08.052
19. G. Gusmano, P. Labella, G. Montesperelli, A. Privitera, S. Tassinari, *Corrosion.* **2006**, *62,* 576–583. **DOI:**10.5006/1.3280671
20. H. Ashassi-Sorkhabi, A. Kazempour, Z. Frouzat, *J. Adhes. Sci. Technol.* **2020**, 1–21. **DOI:**10.1080/01694243.2020.1794357
21. X. Zhang, F. Wang, Y. He, Y. Du, *Corros. Sci.* **2001**, *43*, 1417–1431. **DOI:**10.1016/S0010-938X(00)00160-8
22. S. Ghareba, S. Omanovic, *Corros. Sci.* **2010**, *52,* 2104–2113. **DOI:**10.1016/j.corsci.2010.02.019
23. H. DeryaLeçe, K. C. Emregül, O. Atakol, *Corros. Sci.* **2008,** *50,* 1460–1468. **DOI:**10.1016/j.corsci.2008.01.014
24. I. B. Onyeachu, I. B. Obot, A. A. Sorour, M. I. Abdul-Rashid, *Corros. Sci.* **2019**, *150,* 183–193. **DOI:**10.1016/j.corsci.2019.02.010
25. L. Toukal, S. Keraghel , F. Benghanem, A. Ourari, *Int. J. Electrochem. Sci.* **2018,** *13,* 951–974. **DOI:**10.20964/2018.01.43
26. S. Zafari, A. AsgharSarabi, B. Movassagh, *Asia-Pac. J. Chem. Eng.* **2019**, *14,* e2349. **DOI:**10.1002/apj.2349
27. S. Zafari, A. AsgharSarabi, B. Movassagh, *Coors. Eng. Sci. Technol.* **2020**, *55,* 589–601. **DOI:**10.1080/1478422X.2020.1766863
28. M. Bozorg, M. Rezaeivala, S. Borghei, M. Darroudi, *Thin Solid Films.* **2022**, *762,* 139558. **DOI:**10.1016/j.tsf.2022.139558
29. H. Hakimi, S. Karimi, M. Rezaeivala, *Thin Solid Films.* **2024**, *800*, 140390. **DOI:**10.1016/j.tsf.2024.140390
30. M. Rezaeivala, M. Bozorg, N. Rafiee, K. Sayin, B. Tuzun, *Inorg. Chem. Commun.* **2023**, *148*, 110323. **DOI:**10.1016/j.inoche.2022.110323
31. Z. Rouifi, M. Rbaa , A. S. Abousalem, F. Benhiba, T. Laabaissi, H. Oudda, B. Lakhrissi, A. Guenbour, I. Warad, A. Zarrouk, *Surf. Interfaces.* **2020**, *18,* 100442. **DOI:**10.1016/j.surfin.2020.100442
32. M. Yadav, S. Kumar, T. Purkait, L.O. Olasunkanmi, I. Bahadur, E.E. Ebenso, *J. Mol. Liq.* **2016**, *213,* 122–138. **DOI:**10.1007/s40735-018-0215-3
33. O. Fergachi, F. Benhiba, M. Rbaa, M. Ouakki, M. Galai, R. Touir, B. Lakhrissi, H. Oudda, M. Ebn Touhami, *J. Bio- Tribo-Corros.* **2019**, *5*, 1–13. **DOI:**10.1007/s40735-018-0215-3
34. S. Pournazari, M. H. Moayed, M. Rahimizadeh, *Corros. Sci.* **2013**, *71,* 20–31. **DOI:**10.1016/j.corsci.2013.01.019
35. S. Mouzali, D. Haffar, L. Bouzidi, Z. Bouanane, *J. Electrochem. Sci.* **2017**, *12,* 1042–1063. **DOI:**10.20964/2017.11.65
36. D. K. Dey, M. K. Saha, M. K. Das, N. Bhartiya, R. K. Bansal, G. Rosair, S. Mitra, *Polyhedron.* **1999**, *18,* 2687–2696. **DOI:**10.1016/S0277-5387(99)00171-0
37. I. B. Obot, K. Haruna, T. A. Saleh, *Arab. J. Sci. Eng.* **2019**, *44,* 1–32. **DOI:**10.1007/s13369-018-3605-4
38. C. Lee, W. Yang, R. G. Parr, *Phys. Rev. B.* **1988**, *37*, 785–789. **DOI:**10.1103/PhysRevB.37.785
39. M. Frisch, G. W. Trucks, H. B. Schlegel, G. E. Scuseria, Gaussian 09. Revision d. 01, Gaussian Inc. Wallingford. CT. **2009**.
40. W. Kohn, L. J. Sham, *Phys. Rev A.* **1965***, 137,* 1697–1705. **DOI:**10.1103/PhysRev.137.A1697
41. M. Arivazhagan, V.P. Subhasini, *Spectrochim. Acta. Part A.* **2012**, *91*, 402–410. **DOI:**10.1016/j.saa.2012.02.018
42. M. S. Masoud, A. E. Ali, M. A. Shaker, G. S. Elasala, *Spectrochim. Acta. Part A.* **2012**, *90,* 93–108. **DOI:**10.1016/j.saa.2012.01.028
43. X. R. Mahboub, *Mol. Simul.* **2020**, *46*, 207–212. **DOI:**10.1080/08927022.2019.1690143
44. R. Padash, M. RahimiNasrabadi, A. Shokuhi Rad, A. SobhaniNasab, T. Jesionowski, H. Ehrlich, *Appl. Phys.* **2019**, *125,* 1–11. **DOI:**10.1007/s00339-018-2376-9
45. V. S. Sastri, J. R. Perumareddi, *Corrosion.* **1997**, *53,* 617–622. **DOI:**10.5006/1.3290294
46. N. Metropolis, A. W. Rosenbluth, M. N. Rosenbluth, A. H. Teller, *J. Chem. Physics.* **1953**, *21,* 1087–1092. **DOI:**10.1063/1.1699114
47. F. El-Hajjaji, M. E. Belghiti, B. Hammouti, S. Jodeh, O. Hamed, H. Lgaz, R. Salghi, *Port. Electrochim. Acta.* **2018**, *36*, 197–212. **DOI:**10.4152/pea.201803197
48. P. Crews, J. Rodriguez, M. Jaspars, organic structure analysis, Oxford University Press Inc, New York. **1998**.
49. B. Kumar, K. Smita, B. Kumar, L. Cumbal, *J. Chem. Sci.* **2014,** *126,* 1831–1840. **DOI:**10.1007/s12039-014-0662-4
50. N. Soltani, M. Behpour, S. M. Ghoreishi, H. Naeimi, *Corros. Sci.* **2010**, *52,* 1351–1361. **DOI:**10.1016/j.corsci.2009.11.045
51. I. Jirjees, S. A. Ali, H. A. Mahdi, *Int. J. Sci. Eng. Res.* **2015**, *6,* 735–743.
52. F. El-Hajjaji, I. Merimi, L. ElOuasif, M. ElGhoul, R. Achour,

B. Hammouti, M. E. Belghiti, D. S. Chauhan, M. A. Quraishi, *Port. Electrochim. Acta.* **2019**, *37,* 131–145. **DOI:**10.4152/pea.201903131
53. R.M. Silverstein, F.X. Webster, D.J. Kiemle, seventhed. John-Wiley&Sons, Inc. New York. **2005**.
54. M. Prajila, A. Joseph, *J. Mol. Liq.* **2017**, *241,* 1–8. **DOI:**10.1016/j.molliq.2017.05.136
55. M. Corrales-Luna, T. Le Manh, M. Romero-Romo, M. Palomar-Pardavé, E. M. Arce-Estrada, *Corros. Sci.* **2019**, *153,* 85–99. **DOI:**10.1016/j.corsci.2019.03.041
56. A. Belakhdar, H. Ferkous, S. Djellali, R. Sahraoui, H. Lahbib, Y. Ben Amor, *Mater. Biomater. Sci.* **2020**, *03,* 046–053.
57. F. Abdollahi, M. M. Foroughi, M. Shahidi Zandi, M. Kazemipour, *J. Prog. Color Colorants. Coat.* **2020**, *13,* 155–165. **DOI:**10.30509/pccc.2020.81626.
58. Z. Golshani, S. M. A. Hosseini, M. Shahidizandi, M. J. Bahrami, *Mater. Corros.* **2019**, 1–10. **DOI:**10.1002/maco.201910896.
59. J. Cruz, R. Martinez, J. Genesca, E. Garcia-Ochoa, *J. Electroanal. Chem.* **2004**, *566*, 111–121. **DOI:**10.1016/j.jelechem.2003.11.018
60. K. F. Khaled, *Electrochim. Acta***. 2008**, *53,* 3484–3492. **DOI:**10.1016/j.electacta.2007.12.030
61. H. Zarrok, H. Oudda, A. El Midaoui, A. Zarrouk, B. Hammouti, M. EbnTouhami, A. Attayibat, S. Radi, R. Touzani, *Res. Chem. Interm.* **2008**, *38*, 2051–2063. **DOI:**10.1007/s11164-012-0525-x
62. J Aljourani, K. Raeissi, M . A. Golozar, *Corros. Sci.* **2009**, *51*, 1836–1843. **DOI:**10.1016/j.corsci.2009.05.011
63. A. Döner, R. Solmaz, M. Özcan, G. Kardas, *Corros. Sci.* 2011, *53,* 2902–2913. **DOI:**10.1016/j.corsci.2011.05.027
64. M. A. Hegazy, M. Abdallah, M. K. Awad, M. Rezk, *Corros. Sci.* **2014**, *81*, 54–64. **DOI:**10.1016/j.corsci.2013.12.010
65. T. Tsuru, S. Haruyama, B. Gijutsu, *J. Japan Soc. Corros. Eng.* **1978**, *27,* 573–581. **DOI:**10.3323/jcorr1974.27.11_573
66. G. I. Ramírez-Peralta, U. León-Silva, M. E. NichoDíaz, M. G. Valladares-Cisneros, *Mater. Corros.* **2018**, *69*, 1631–1637. **DOI:**10.1002/maco.201810119
67. A. Y. Musa, R. T. T. Jalgham, A. B. Mohamad, *Corros. Sci.* **2012**, *56*, 176–183. **DOI:**10.1016/j.corsci.2011.12.005
68. C. Bataillon, S. Brunet, *Electrochimica. Acta.* **1994**, *39,* 455–465. **DOI:**10.1016/0013-4686(94)80086-3
69. H. Elattari, K. Chefira, M. Siniti, A. El kihel, H. Rchid, *Int. J. Rec. Tren. Eng. Res.* **2017**, *03,* 167–179. https://www.researchgate.net/publication/342349705.
70. I. Ahamad, R. Prasad, M. A. Quraishi, *Corros. Sci.* **2010**, *52,* 1472–1481. **DOI:**10.1016/j.corsci.2010.01.015
71. H. J. Guadalupe, E. García-Ochoa, P. J. Maldonado-Rivas, J. Cruz, T. Pandiyan, *J. Electroanal. Chem,* **2011**, *655,* 164–172. **DOI:**10.1016/j.jelechem.2011.01.039
72. A. O Yüce, B. D. Mert, G. Kardaş, B. Yazici, *Corros. Sci.* **2014***, 83,* 310–316. **DOI:**10.1016/j.corsci.2014.02.029
73. B. Liu, H. Xi, Z. Li Q. Xia, *Appl. Surf. Sci.* **2012**, *258,* 6679–6687. **DOI:**10.1002/ejoc.201200648
74. F. M. Donahue, K. Nobe, *J. Electrochem. Soc.* **1965**, *112,* 886–89. **DOI:**10.1149/1.2423723
75. M. Srivastava, P. Tiwari, S. K. Srivastava, R. Prakash, G. Ji, *J. Mol. Liq.* **2017**, *236,* 184–197. **DOI:**10.1016/j.molliq.2017.04.017
76. A. Dutta, S. S. Panja, M. M. Nandi, D. Sukul, *J. Chem. Sci.* **2015**, *127,* 921–929. **DOI:**10.1007/s12039-015-0850-x
77. W. Durnie, R.D. Marco, A. Jefferson, B. Kinsella, *J. Electrochem. Soc.* **1999**, *146,* 1751–1756. **DOI:**10.1149/1.1391837
78. P. Rugmini Ammal, R. P. Anupama, K. Ramya, J. Sam, J. Abraham, *J. Adhes. Sci. Technol.* **2019**, 1–23. **DOI:**10.1080/01694243.2019.1637169
79. L. j .M. Vračar, D. M. Dražić, *Corros. Sci.* 2002, *44,* 1669–1680. **DOI:**10.1016/S0010-938X(01)00166-4
80. A. O. Yüce, G. Kardaş, *Corros. Sci.* **2012**, *58,* 86–94. **DOI:**10.1016/j.corsci.2012.01.013
81. A. E. Stoyanova, E. I. Sokolova, S. N. Raicheva, *Corros. Sci.* **1997**, *39,* 1595–1604. **DOI:**10.1016/S0010-938X(97)00063-2
82. A. S. Fouda, S. S. Elkaabi, A. K. Mohamed, *Anti-Corros. Methods Mater.* **1989**, *36,* 9–12. **DOI:**10.1108/eb020787
83. M. J. Bahrami, S. M. A. Hosseini, P. Pilvar, *Corros. Sci.* **2010**, *52,* 2793–2803. **DOI:**10.1016/j.corsci.2010.04.024
84. O. Radovic, Proc. 7th European Symposium on Corrosion Inhibitors, Ann. Univ. Ferrara Italy. **1990**, p330.
85. H. Jafari, I. Danaee, H. Eskandari, M. Rashvand Avei, *J. Mater. Sci. Technol.* **2014**, *30,* 239–252. **DOI:**10.1016/j.jmst.2014.01.003
86. K. M. Hijazi, A. M. Abdel-Gaber, G. O. Younes, *Int. J. Electrochem. Sci.* **2015**, *10*, 4366– 4380. **DOI:**10.1016/S1452-3981(23)06629-4
87. M. Dahmani, A. Et-Touhami, S. S. Al-Deyab, B. Hammouti, A. Bouyanzer, *Int. J. Electrochem. Sci.* **2010**, *5*, 1060–1069. **DOI:**10.1016/S1452-3981(23)15344-2
88. K. C. Emregül, M. Hayvalí, *Corros. Sci.* **2006**, *48,* 797–812. **DOI:**10.1016/j.corsci.2005.03.001
89. A. S. El-Tabei, M. A. Hegazy, A. H. Bedair, M. A. Sadeq, *J. Surfact. Deterg.* **2014**, *17,* 341–352. **DOI:**10.1007/s11743-013-1524-7
90. L. Tang, G. Mu, G. Liu, *Corros. Sci.* 2003, *45,* 2251–2262. **DOI:**10.1016/S0010-938X(03)00046-5
91. W. Li, X. Zhao, F. Liu, B. Hou, *Corros. Sci.* **2008**, *50*, 3261–3266. **DOI:**10.1016/j.corsci.2008.08.015
92. H. Ashassi-Sorkhabi, B. Shaabani, D. Seifzadeh, *Electrochim. Acta.* **2005**, *50,* 3446–3452. **DOI:**10.1016/j.electacta.2004.12.019
93. R. Kooliyat, J. T. Kakkassery, V. P. Raphael, S. V. Cheruvathur, B. M. Paulson, *Int. J. Electrochem.* **2019**, 1–13. **DOI:**10.1155/2019/1094148
94. M. Eissa, S. H. Etaiw, E. E. El-Waseef, A. El-Hossiany, A. S. Fouda, *Sci. Rep.* **2024,** *14,* 2413. **DOI:**10.1038/s41598-024-51576-9
95. A. S. Fouda, S. E. H. Etaiw, D. M. Abd El-Aziz, A. A. El-Hossiany, U. A. Elbaz,. *BMC Chem.* **2024**, *18*, 21. **DOI:**10.1186/s13065-024-01121-6
96. M. M. Kabanda, L. C. Murulana, M. Ozcan, F. Karadag, I. Dehri, I. B. Obot, E. E. Ebenso, *Int. J. Electrochem. Sci***. 2012**, *7*, 5035–5056. **DOI:**10.1016/S1452-3981(23)19602-7
97. L. M. Rodríguez-Valdez, W. Villamisar, M. Casales, J. G. Gonzalez-Rodriguez, A. Martınez-Villafane, L. Martinez, D.

Glossman-Mitnik, *Corros. Sci.* **2006**, *48,* 4053–4064. **DOI:**10.1016/j.corsci.2006.05.036
98. S. Martinez, I. Štagljar, *J. Mol. Struct.* **2003**, *640,* 167–174. **DOI:**10.1016/j.theochem.2003.08.126
99. M. A. Amin, K. F. Khaled, S. A. Fadl-Allah, *Corros. Sci.* **2010**, *52,* 140–151. **DOI:**10.1016/j.corsci.2009.08.055
100. Aouniti, H. Elmsellem, S. Tighadouini, M. Elazzouzi, S. Radi, A. Chetouani, B. Hammouti, A. Zarrouk, *J. Taibah. Univ. Sci*. **2016**, 774–785. **DOI:**10.1016/j.jtusci.2015.11.008
101. M. Behpour, S. M. Ghoreishi, N. Soltani, M. Salavati-Niasari, *Corros. Sci.* **2009**, *51*, 1073–1082. **DOI:**10.1016/j.corsci.2009.02.011
102. I.B . Obot, D. D Macdonald, Z. M. Gasem, *Corros. Sci.* **2015**, *99,* 1–30. **DOI:**10.1016/j.corsci.2015.01.037
103. F. Mohsenifar, H. Jafari, K. Sayin, *J. Bio. Tribo. Corros.* **2016**, *2,* 1–13. **DOI:**10.1007/s40735-015-0031-y
104. I. Lukovits, E. Klaman, F. Zucchi, *Corrosion.* **2001**, *57,* 3–8. **DOI:**10.5006/1.3290328
105. N. Kovačević, A. Kokalj, *Corros. Sci* **2011**, *53,* 909–921. **DOI:**10.1016/j.corsci.2010.11.016
106. B. Xu, W. Gong, K. Zhang, W. Yang, Y. Liu, X. Yin, H. Shi, Y. Chen, *J. Taiwan. Inst. Chem. Eng.* **2015**, *51,* 193–200. **DOI:**10.1016/j.jtice.2015.01.014
107. N. Okulik, A. H. Jubert, *J. Mol. Des.* **2005**, *4,* 17–30. **DOI:**10.1016/S0398-0499(05)74818-6.
108. H. Tian, W. Li, K. Cao, B. Hou, *Corros. Sci.* **2013**, *73,* 281–291. **DOI:**10.1016/j.corsci.2013.04.017
109. M. ElBelghiti, Y. Karzazi, A. Dafali, B. Hammouti, F. Bentiss, I. B. Obot, I. Bahadur, E. E. Ebenso, *J. Mol. Liq.* **2016**, *218,* 281–293. **DOI:**10.1016/j.molliq.2016.01.076
110. S. Peljhan, A. Kokalj, *Phys. Chem. Chem. Phys.* **2011,** *13,* 20408–20417. **DOI:**10.1039/c1cp21873e

Povzetek

Sintetizirali in karakterizirali smo novo heterociklično Schiffovo bazo: 4-(1-(4-(dimetilamino)benzil)-5-metil-1*H*-benzo[d]imidazol-2-il)-*N*,*N*-dimetilanilin (L). Molekularno strukturo spojine L smo določili z metodami ^{1}H NMR, FT-IR, UV-Vis spektroskopijo in elementno analizo. Učinkovitost in mehanizem inhibicije spojine L proti koroziji ogljikovega jekla v 1 M HCl in 0,5 M H_2SO_4 smo preučevali z metodo izgube mase ter z elektrokemijskimi tehnikami (Tafelova polarizacija in elektrokemijska impedančna spektroskopija, EIS). Rezultati, pridobljeni s temi metodami, so pokazali, da se z naraščajočo koncentracijo spojine L povečuje tudi njena inhibicijska učinkovitost (η %) ki doseže 82,85 % pri 25 °C in koncentraciji 1×10^{-2} M. Po drugi strani pa je η padla na 75,25 % pri isti koncentraciji in temperaturi 55 °C. Polarizacijske krivulje kažejo, da se spojina obnaša kot inhibitor mešanega tipa. Ugotovili smo, da adsorpcija te spojine sledi Langmuirovi adsorpcijski izotermi. Morfologija površine ogljikovega jekla po delovanju spojine L, pridobljena s pomočjo vrstične elektronske mikroskopije (SEM) in mikroskopije na atomsko silo (AFM), je potrdila, da se je spojina L adsorbirala na površino ogljikovega jekla ter tvorila zaščitni film. Izračunali smo kinetične in termodinamske parametre. Z metodo teorije gostotnih funkcionalov (DFT) smo določili tudi kvantno-kemijske parametre. Študija potrjuje ujemanje med eksperimentalnimi in teoretičnimi rezultati.